



Nonlinear effects of actuator rate and acceleration limits on closed-loop systems: a describing function approach

Luca Marino¹ · Jurij Sodja¹

Received: 16 September 2025 / Revised: 20 January 2026 / Accepted: 3 March 2026
© The Author(s) 2026

Abstract

Actuator nonlinearities can significantly affect control systems, leading to performance degradation and even loss of stability. Physical constraints such as rate and acceleration limits are particularly detrimental in applications where rapid actuation is required, yet their combined effects remain largely unexplored. This paper investigates the nonlinear dynamic behaviour induced by rate and acceleration limits in closed-loop systems, focusing on their steady-state response to sinusoidal excitation. The saturation regimes associated with these nonlinearities are fully characterised, and their analytical boundaries are represented in a two-dimensional parameter space defined by normalised rate and acceleration limits. Sinusoidal describing functions are derived for each regime, providing a unified frequency-domain representation of the actuator dynamics. These formulations are employed to analyse the impact of actuator nonlinearities on closed-loop dynamics, including the onset of nonlinear behaviour, phase lag and gain reduction. Analytical conditions for the occurrence of jump resonance are derived, along with the lowest frequency where multiple steady-state solutions appear, leading to potential abrupt changes in system response. The applicability of the proposed framework is demonstrated through both an illustrative first-order system and a realistic high-order aeroservoelastic model for gust load alleviation, where the interaction between actuator nonlinearities and closed-loop dynamics is shown to produce multiple jump resonance scenarios and isolated nonlinear response branches. The results highlight the critical role of actuator rate and acceleration limits in high-bandwidth control applications and provide practical insights for frequency-domain stability assessment and preliminary feedback control system design.

Keywords Actuator nonlinearities · Aeroservoelastic systems · Feedback control systems · Gust load alleviation · Jump resonance

1 Introduction

Actuators are critical components in control systems, serving as the interface between command signals and physical motion. Modern engineering applications often rely on high-performance actuators to execute rapid and precise commands. However, real actuators are constrained by physical limitations, such as amplitude, rate and acceleration saturation, as well as by other mechanical nonlinearities, including backlash, free-play and friction. These nonlinearities are often overlooked in early design phases, but can significantly impact the performance and stability of control systems when active.

Actuator nonlinearities affect applications across several engineering domains. In civil structures, including buildings [1, 2] and offshore platforms [3], actuator saturation can limit the performance of vibration control and attenuation systems. In automotive systems, active suspensions and braking controllers are frequently constrained by actuator dynamics and delays [4, 5]. In unmanned spacecraft [6] and underwater vehicles [7], thruster saturation and rate limits can reduce the effectiveness of fault-tolerant controllers. Actuator saturation can also lead to poor tracking performance in robotic devices [8]. In aerospace systems, nonlinear behaviour of flight control surface actuators is a well-known source of performance degradation and dynamic instabilities. Actuator rate limitations, due to their impact on the phase lag in closed-loop systems, can lead to pilot-induced oscillations (PIOs) of type II [9, 10], which caused the fatal JAS39 Gripen [11, 12] and YF-22 accidents [13]. In current days, frequency-dependent actuator nonlinearities, such as rate and acceleration limits,

✉ Luca Marino
l.marino-1@tudelft.nl

¹ Department of Aerospace Structures and Materials, Delft University of Technology, Kluyverweg 1, Delft 2629, HS, The Netherlands

are particularly critical for closed-loop flight control functions, including gust load alleviation [14, 15] and active flutter suppression [16], where high-frequency performance is required to deal with fast transients and flow variations. Nonetheless, in state-of-the-art control law design, actuator nonlinearities are often neglected [15] and linearised models with sufficiently high robustness margins are instead considered [17, 18].

This paper focuses on the analysis of the nonlinear effects caused by actuator rate and acceleration limits in the dynamic response of closed-loop control systems. Rate saturation can occur in any actuation system due to its limited rate of travel. When the demanded velocity exceeds the rate limit, the actual actuator deflection will have a reduced amplitude and lag behind the input signal. This can either be caused by the input amplitude or frequency, rendering rate limit a non-static nonlinearity [15]. In hydraulic actuators, rate saturation occurs when the main control valve reaches its maximum flow capability [19]. Differently, in electro-mechanical actuators, achievable velocity is mostly determined by bearings and power source limitations [14, 15]. Acceleration limit is also a common physical limitation in actuators. The maximum achievable acceleration is limited by the maximum force or torque available in the system, which is usually determined by mechanical and electrical constraints, such as motor capacity [14, 15] and servo valve limits [19]. In several applications, rate limit functions are also imposed in the control laws to limit the commanded actuator rate, aiming to protect the system from excessive commands and physical wear, and to avoid unwanted dynamic behaviour [19, 20]. In their investigation on the nonlinear behaviour of hydraulic actuation systems, Fielding and Flux [19] underline how acceleration limits should be accurately modelled to avoid undesired dynamic behaviour, while Tang et al. [14, 15] concluded that the effect of the acceleration limit is, along with backlash, more severe than that of other actuator nonlinearities (including deflection and rate limits, and dead time) when dealing with the closed-loop gust load alleviation aeroservoelastic systems. Nonetheless, in contrast to actuator saturation and rate limit, the acceleration limit nonlinearity has received little attention in the literature, and the combined effect of rate and acceleration limits is mostly unexplored.

The theoretical analysis of rate-limited systems is often carried out by using sinusoidal describing functions. A describing function is an approximate frequency response function, which describes the relationship between the input and output of a nonlinearity in the frequency domain [21, 22], and can be used to assess the effect of a single dominant nonlinearity, or a combination of nonlinearities, on the stability and robustness of a feedback loop [19]. In closed-loop systems, describing functions are primarily used to determine the potential onset of limit cycle oscillations (LCOs); further applications include the prediction of subharmonics,

jump phenomena, and the response of nonlinear systems to sinusoidal inputs [23]. The main assumptions required for the validity of the describing function analysis are the time-invariance of the nonlinear element, and the presence of a dominant nonlinearity (or group of nonlinearities) [21]. In addition, the describing function is most effective when the underlying linear system does not exhibit high-frequency resonances, which could otherwise amplify higher-order harmonic components [19, 21]. Nonlinearities such as rate and acceleration limits respect these assumptions, and increase the reliability of the analysis by acting as low-pass filters, therefore attenuating the high-frequency content of the linear element of the system. In the literature, describing functions were often used to investigate the effect of the rate limit. Hanke [24] developed the describing function of the rate limit for the analysis of the handling qualities of the open- and closed-loop systems in frequency domain, and the determination of the onset frequency of the rate limit nonlinearity from input amplitude and frequency. Describing function analysis was also used by Fielding and Flux [19] to investigate the stability and robustness of a closed-loop systems with a rate limiting element, with a particular focus on the prediction of LCOs induced by the nonlinearity in flight control systems. In the same publication, the effect of an acceleration limiting element were also addressed, deriving a linear approximation capable of describing the dynamic behaviour at high frequencies. While previous work only focused on the behaviour of rate-limited systems in full saturation regimes, i.e., when the rate limit fully saturates the sinusoidal input producing a triangle wave output, Roman and Ponce [25] derived a closed-form analytical formulation also for those cases where the rate limit only partially saturate the sinusoidal input. The same authors also addressed the evaluation of the accuracy of the rate limit describing function compared to numerical integration [25], and investigated the effect of rate limiters in feedback loops along with an open-loop unstable linear plant [26]. In recent years, Tavakkoli *et al.* [27] performed the stability analysis of a closed-loop second-order system with a rate-limited input using an approach based on describing function method. Approaches based on the describing function have also been used in many studies aimed to the design of rate limit compensation methods [20, 28–30].

Several researchers investigated the role of the rate limit in the onset of PIOs (see, e.g., [10, 31]). In particular, Gilbreath derived an equivalent describing function able to describe the frequency response of closed-loop rate-limited systems, determining the open-loop onset point (OLOP) stability boundary, according to a procedure first introduced by Duda [9], and observing the presence of sudden nonlinear jumps in the system's response. Jump resonance is a well-known phenomenon associated with fold bifurcations and the coexistence of multiple steady-state solutions in nonlinear feedback systems [32]. While the possibility of investigating

jump resonances via describing function analysis is well-documented (see, e.g., [21, 33]), only limited evidence is available for its presence and effects in rate-limited systems. Moreover, the describing function of closed-loop systems with acceleration limits, or combined rate and acceleration limits, is mostly unexplored.

Despite extensive research on rate-limited systems, comparatively little attention has been devoted to acceleration limits, and the combined effects of rate and acceleration limits on closed-loop dynamics remain not well understood. This is partly because acceleration constraints are often implicitly embedded within linear actuator dynamics, such as finite bandwidth or second-order models, and may therefore remain concealed unless the actuator operates near its force or torque limits. However, modern closed-loop flight control applications, such as gust load alleviation, demand high bandwidth and fast response, making the explicit consideration of combined rate-acceleration limitations necessary for an accurate dynamic analysis (see, e.g., [14, 15]).

In this paper, the nonlinear effects induced by actuator rate and acceleration limits on the dynamic behaviour of closed-loop systems are investigated by means of a describing function analysis. The steady-state actuator response to sinusoidal input is first explored to identify and characterise the saturation regimes determined by these nonlinearities. Complete analytical formulations are then derived for the describing function of combined rate and acceleration limits for each saturation regime. The analysis of closed-loop systems containing rate and acceleration limit nonlinear elements is finally conducted using the derived describing functions, enabling the evaluation of the onset frequency of nonlinear behaviour and the investigation of the approximate nonlinear response of the feedback loop, including the characterisation of nonlinear jump resonances. The proposed framework is applied to both an illustrative first-order system and a realistic high-order aeroservoelastic control system for gust load alleviation, in order to demonstrate its applicability to practical high-bandwidth control problems.

The paper is organised as follows. The investigation of the actuator saturation regimes under sinusoidal input is presented in Sect.2. In Sect.3, analytical describing functions are derived for rate and acceleration limits, and for combined rate and acceleration limit nonlinearities. The application of the describing functions to the analysis of closed-loop systems is addressed in Sect.4, while their use in the analysis of a high-order aeroservoelastic gust load alleviation system is presented in Sect.5. Concluding remarks are provided in Sect.6.

A preliminary version of this study was presented at the International Forum on Aeroelasticity and Structural Dynamics (IFASD 2024) [34]. That work provided an initial describing function formulation for actuators with combined rate and acceleration limits. The present paper substantially

extends that preliminary study by: (i) providing a generalised nonlinear analysis framework for closed-loop systems; (ii) deriving analytical conditions for the occurrence of jump resonance and the corresponding bifurcation frequencies; (iii) demonstrating the proposed analysis on a realistic high-order aeroservoelastic model, highlighting the effects of actuator rate and acceleration limits on closed-loop aeroelastic dynamics.

2 Actuator saturation regimes for sinusoidal input

The first step towards deriving an analytical formulation for the describing functions of rate and acceleration limits is the characterisation of the different saturation regimes introduced by these nonlinearities. Since sinusoidal describing functions are obtained by considering the fundamental harmonic of the nonlinear response to sinusoidal input at each frequency, this section focuses on the steady-state actuator response to a sinusoidal excitation, first considering the cases where only one of the rate or acceleration limits is active, and then the case of combined rate and acceleration limits.

2.1 Rate limit

Let us first denote the actuator input and output signals as $x(t)$ and $y(t)$, respectively, and assume that the rate limit R_V is applied by the actuator on the output signal, such that

$$|\dot{y}(t)| \leq R_V. \quad (1)$$

If the signal

$$x(t) = x_0 \cos(\omega t) \quad (2)$$

is given as an input to the actuator, the rate limit will only be effective if the amplitude of the input rate exceeds R_V , i.e., if

$$R_V < \omega x_0; \quad (3)$$

otherwise, no saturation will occur and the output signal will be unaffected by the rate limit. In this context, it is useful to introduce a non-dimensional parameter called *rate limit ratio* to indicate the ratio between the rate limit value and the maximum input rate

$$r_V = \frac{R_V}{\omega x_0}. \quad (4)$$

According to the above definition, the rate limit is only effective when $r_V < 1$. In this case, three different types

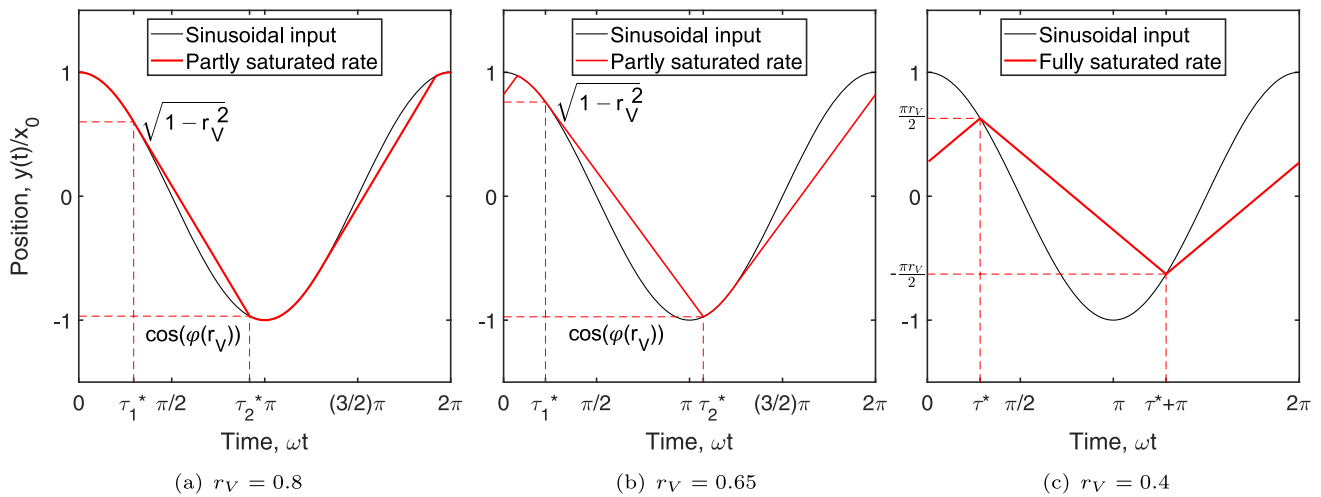


Fig. 1 Steady-state response of a rate-limited actuator to sinusoidal input

of saturation regimes can occur in the steady-state actuator response, as shown in Fig. 1 partial saturation, without (Fig. 1a) or with amplitude reduction (Fig. 1b), and full saturation (Fig. 1c).

Partial saturation is the first regime observed as the rate limit ratio is decreased below unity. When the rate limit is only slightly larger than the maximum input rate, the time interval where saturation occurs is entirely included within the half-period between a maximum and the subsequent minimum (and vice versa) of the sinusoidal input; therefore, the maximum value of the steady-state response remains unaltered, as visible in Fig. 1a. To minimise the number of parameters required for describing the properties of the steady-state actuator response, it is convenient to refer to the non-dimensional time $\tau = \omega t$. Input and output signals are also normalised by the input amplitude. It follows that the signal rate is normalised by ωx_0 ; therefore, based on Eq.(4), the normalised rate limit coincides with the rate limit ratio. In general, the notation \bar{g} is used to refer to a signal g normalised by x_0 , while the symbol ' will be used to indicate derivatives with respect to the non-dimensional time τ .

Denoting as $\tau \in [0, 2\pi]$ the non-dimensional time interval representing one period of the input signal in steady-state conditions, let us determine the starting and ending times of the rate saturation interval, as well as the corresponding actuator position values. The time τ_1^* where saturation first occurs can easily be determined as the time instant where the amplitude of the normalised input velocity $\bar{x}' = -\sin(\tau)$ equates the normalised rate limit r_V . The condition

$$|\bar{x}'(\tau_1^*)| = r_V \quad (5)$$

yields

$$\tau_1^* = \sin^{-1}(r_V), \quad (6)$$

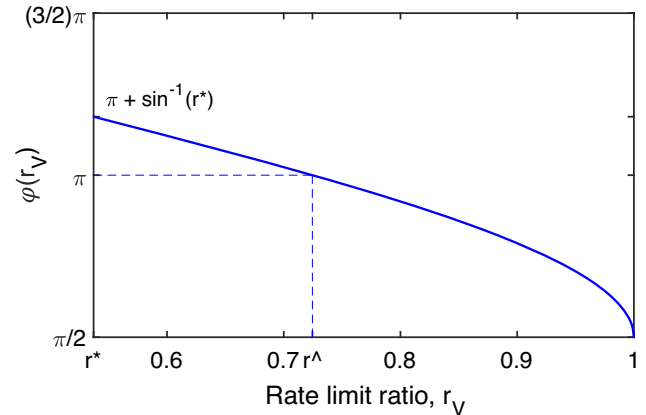


Fig. 2 Non-dimensional saturation ending time in partial rate saturation regime as a function of the rate limit ratio

as the smallest solution in the interval $[0, 2\pi]$. Substituting τ_1^* into the above expression of the input rate, and considering that $\bar{x}(\tau_1^*) = \bar{y}(\tau_1^*)$, it is obtained that

$$\bar{x}_1^* = \bar{y}_1^* = \sqrt{1 - r_V^2}. \quad (7)$$

As visible in Fig. 1a, output saturation terminates when the rate limited output intersects the sinusoidal input, at $\tau = \tau_2^*$. Let us introduce the function φ of the rate limit ratio such that $\tau_2^* = \varphi(r_V)$ and $\bar{x}_2^* = \cos(\varphi(r_V))$. Evaluating the intersection between the linear portion of the actuator output, whose equation reads as

$$\bar{y}(\tau) = \sqrt{1 - r_V^2} - r_V(\tau - \tau_1^*), \quad (8)$$

and the input signal $\bar{x}(\tau) = \cos(\tau)$, it is possible to obtain the following implicit analytical expression for $\varphi(r_V)$:

$$r_V \varphi(r_V) + \cos(\varphi(r_V)) = r_V \sin^{-1}(r_V) + \sqrt{1 - r_V^2}. \quad (9)$$

If the saturation ending time is such that $\tau_2^* > \pi$, the maxima of the sinusoidal input will also be saturated, leading to an amplitude reduction in the actuator output (Fig. 1b). The rate limit ratio value r^* for which amplitude reduction first occurs can be determined numerically by solving the equation $\varphi(r_V) = \pi$, and is equal to 0.7246. In this case, the reduced amplitude of the actuator steady-state response will be equal to $-\cos(\varphi(r_V))$.

The transition from partial to full rate saturation occurs when the ending time τ_2^* of the saturation interval coincides with the start of the subsequent saturation interval at $\tau_1^* + \pi$, i.e., when

$$\varphi(r_V) = \pi + \sin^{-1}(r_V). \quad (10)$$

This leads to rate saturation occurring throughout the entire steady-state response. By replacing the above value of $\varphi(r_V)$ into Eq.(9), it results that the transition takes place when the rate limit ratio is equal to

$$r^* = \frac{2}{\sqrt{4 + \pi^2}} \cong 0.5370, \quad (11)$$

as previously reported by several authors (see, e.g., [9, 10]). This value will be referred to as *critical ratio*.

A graphical representation of $\varphi(r_V)$ is provided in Fig. 2, where it can be observed that $\varphi(r_V)$ is a monotonically decreasing function of r_V , attaining its minimum value $\pi/2$ at $r_V = 1$. Equation (9) has been solved numerically for $r_V \in [r^*, 1]$ using the MATLAB function `fzero`, searching for roots within the interval $\varphi(r_V) \in [\pi/2, \pi + \sin^{-1}(r^*)]$. The monotonicity of $\varphi(r_V)$ over this range guarantees the uniqueness of the solution.

The actuator output in full rate saturation regime is characterised by a sequence of linear variations of the position over time (see Fig. 1c), with non-dimensional rate remaining constant at $\pm r_V$; the output signal therefore resembles a triangle wave. The switching between the positive and negative saturated rate occurs across the intersection with the sinusoidal input, at

$$\tau^* = \cos^{-1}\left(\frac{\pi}{2}r_V\right). \quad (12)$$

Given the 2π -periodicity of the response and its rate, it follows that the signal amplitude in this regime is equal to $(\pi/2)r_V$.

2.2 Acceleration limit

Let us now analyse the effect of the acceleration limit R_A , such that

$$|\ddot{y}(t)| \leq R_A, \quad (13)$$

on the actuator output in steady-state conditions, assuming that no rate limit is applied. Since the maximum input acceleration of the sinusoidal signal from Eq.(2) is equal to $\omega^2 x_0$, it is convenient to introduce the *acceleration limit ratio* as

$$r_A = \frac{R_A}{\omega^2 x_0}. \quad (14)$$

In this notation, the acceleration limit will only affect the actuator output if $r_A < 1$. In this case, three saturation regimes can be observed: partial saturation, without (Fig. 3a) or with velocity reduction (Fig. 3b), and full saturation (Fig. 3c). It can be observed that the effect of the acceleration limit on the output velocity is the same as that of the rate limit on the output position. However, this leads to a significantly different actuator output from that induced by the rate limit, as shown in Fig. 4 for the three saturation regimes and discussed in what follows.

In partial acceleration saturation regime, the actuator steady-state response presents a parabolic evolution in those time intervals where the acceleration is saturated. The output position therefore consists of a sequence of sinusoidal and parabolic traits (see, e.g., Fig. 4a). Since the maximum acceleration in the sinusoidal input occurs at the maximum deflection (in absolute value), amplitude reduction is observed in the actuator output for any acceleration saturation regime. Therefore, unlike the rate limit, the acceleration limit cannot lead to partial saturation regime without amplitude reduction. By extending the results shown in subsection 2.1 to the acceleration limit case, it can easily be derived that the starting and ending times of the saturation interval are $\tau_1^* = \cos^{-1}(-r_A)$ and $\tau_2^* = \varphi(r_A) + \pi/2$.

In full acceleration saturation regime, achieved when the acceleration limit ratio falls below the critical ratio r^* , the steady-state actuator response consists of a sequence of parabolic traits, as shown in Fig. 4c, corresponding to the acceleration switching between r_A and $-r_A$. Exploiting the properties of parabolas and the response symmetry, it can be derived that the response amplitude is equal to $(\pi^2/8)r_A$, while the switch occurs at

$$\tau^* = \pi/2 + \cos^{-1}(r_A). \quad (15)$$

The phase delay introduced by the acceleration limit can here be evaluated as the lag between the input and output maxima, which is equal to $\cos^{-1}(r_A)$.

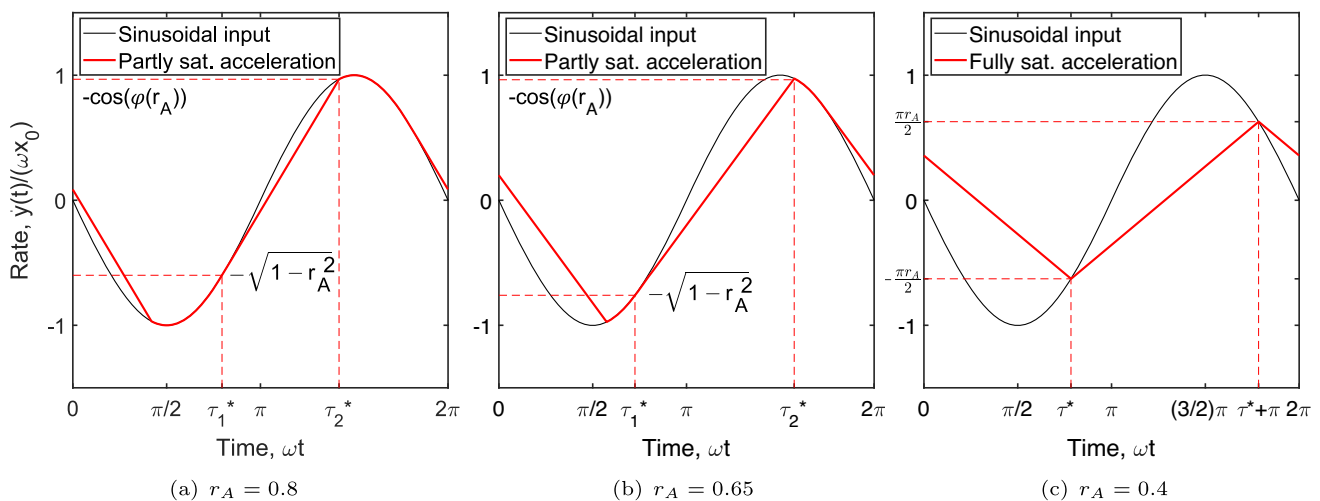


Fig. 3 Steady-state output rate of an acceleration-limited actuator under sinusoidal input

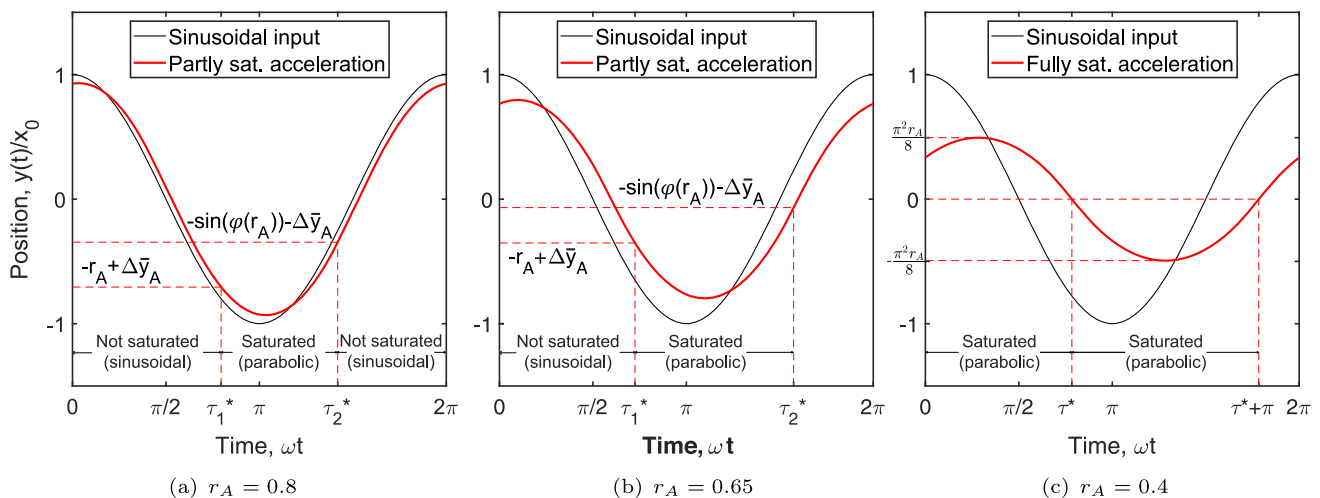


Fig. 4 Steady-state output position of an acceleration-limited actuator under sinusoidal input

2.3 Combined rate and acceleration limit

Let us consider the case of an actuator where the rate and acceleration of the output signal are limited by R_V and R_A , respectively. As discussed in Sect. 1, the presence of combined rate and acceleration limits can be the consequence of physical limitations, including limited power and torque available, or it can be imposed by ad hoc filters (see, e.g., [35, 36]) to prevent the actuator from excessive commanded output which could lead to physical damage. It is important to consider that, when rate saturation occurs, the output rate of the actuator becomes nonsmooth (see Fig. 1), leading to the presence of infinitely large spikes in the output acceleration at the transition times τ_1^* , τ_2^* and τ^* . As a consequence, any finite value of the acceleration limit will affect the actuator output. Conversely, even in the presence of an acceleration limit, no effects from the rate limit will be seen if $r_V \geq 1$;

in this case, the output signal will behave as described in subsection 2.2. Actuator behaviour for $r_V < 1$ is addressed in the following discussion, which is organised by considering three different configurations: (i) full rate saturation ($r_V \leq r^*$) with any acceleration limit; (ii) partial rate saturation ($r^* < r_V < 1$) with acceleration limit $r_A \geq 1$; (iii) partial rate saturation with acceleration limit $r_A < 1$. Transitions among the different saturation regimes, response amplitude and phase delay will be derived and represented in the two-dimensional parameter space defined by r_V and r_A .

2.3.1 Full rate saturation with acceleration limit

In this first case, it is assumed that an acceleration limit is applied along with a rate limit such that $r_V \leq r^*$. In this scenario, the rate limit leads to full saturation, inde-

pendently of the acceleration limit value; therefore, partial saturation is not possible under any circumstances. However, the instantaneous switching between positive and negative rate saturation, represented in Fig. 1c, leads to the presence of discontinuities in the output signal rate, and to infinitely large acceleration peaks. As a consequence, any finite value of the acceleration limit will affect the output signal, eliminating rate discontinuities. Therefore, two different saturation regimes are possible: full mixed saturation, where an alternation of rate and acceleration saturated intervals occurs (see Fig. 5a), or full acceleration saturation only, where no rate saturation is observed, as shown in Fig. 5b.

Full mixed saturation results from the saturation of the acceleration peaks generated by the rate discontinuities. In Fig. 5a, it can be observed that the acceleration saturation interval starts in correspondence of the switch between positive and negative rate saturation, with time instant τ_1^* given by Eq. (12). The saturation ending time τ_2^* can be determined as follows. Since $\bar{y}'(\tau_1^*) = r_V$ and $\bar{y}'(\tau_2^*) = -r_V$ (see Fig. 5a), it can be easily deduced that

$$\Delta\tau_A = \tau_2^* - \tau_1^* = \frac{2r_V}{r_A}. \quad (16)$$

The produced output velocity consists of a trapezoidal wave, oscillating between $\pm r_V$ with slope given by $\pm r_A$, while the position presents an alternation of linear and parabolic traits. The resulting phase delay between the input and output signals can be obtained from Eqs. (12) and (16) and is given by

$$\Delta\tau = \cos^{-1}\left(\frac{\pi}{2}r_V\right) + \frac{r_V}{r_A}. \quad (17)$$

The transition to fully saturated acceleration regime takes place when the value of r_A is such that acceleration is saturated in the whole interval $[\tau_1^*, \tau_2^*]$, i.e., for

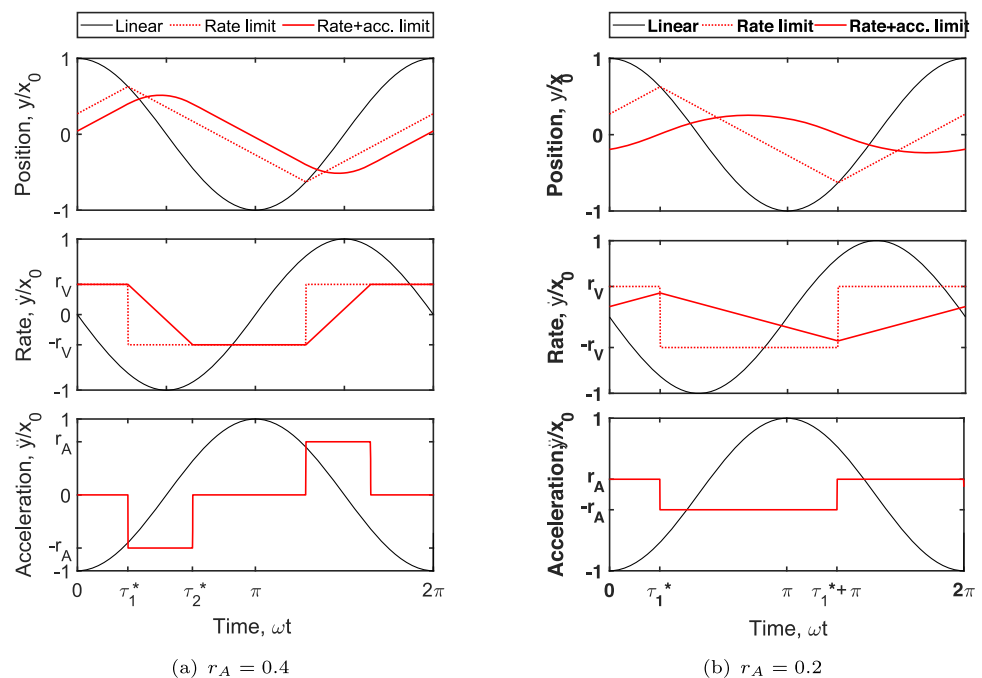
$$r_A = \frac{2}{\pi}r_V. \quad (18)$$

In fact, in this case, the acceleration saturation interval becomes $\Delta\tau_A = \pi$, covering half of the signal period. Further decreases in r_A will only lead to an amplitude reduction of the output position and rate amplitude, which will be equal to $(\pi^2/8)r_A$ and $(\pi/2)r_A$ respectively, as specified in subsection 2.2. However, the switch between positive and negative acceleration saturation occurs in correspondence of the rate saturation switching in the underlying rate limited signal (see Fig. 5b), i.e., at

$$\tau_1^* = \cos^{-1}\left(\frac{\pi}{2}r_V\right), \quad (19)$$

while the phase delay introduced by rate and acceleration limits is equal to $\tau_1^* + \pi/2$. These values differ from those obtained for full acceleration saturation in the absence of rate limit, reported in Eq. (15). It can be concluded that, while a strict acceleration limit can conceal the presence of a rate limit, which does not affect the response amplitude in this saturation regime, the effect from the latter can still be observed in terms of phase delay in the output signal, which is, in this specific case, only dependent on the rate limit ratio.

Fig. 5 Steady-state response of a rate and acceleration-limited actuator to sinusoidal input for $r_V = 0.4$



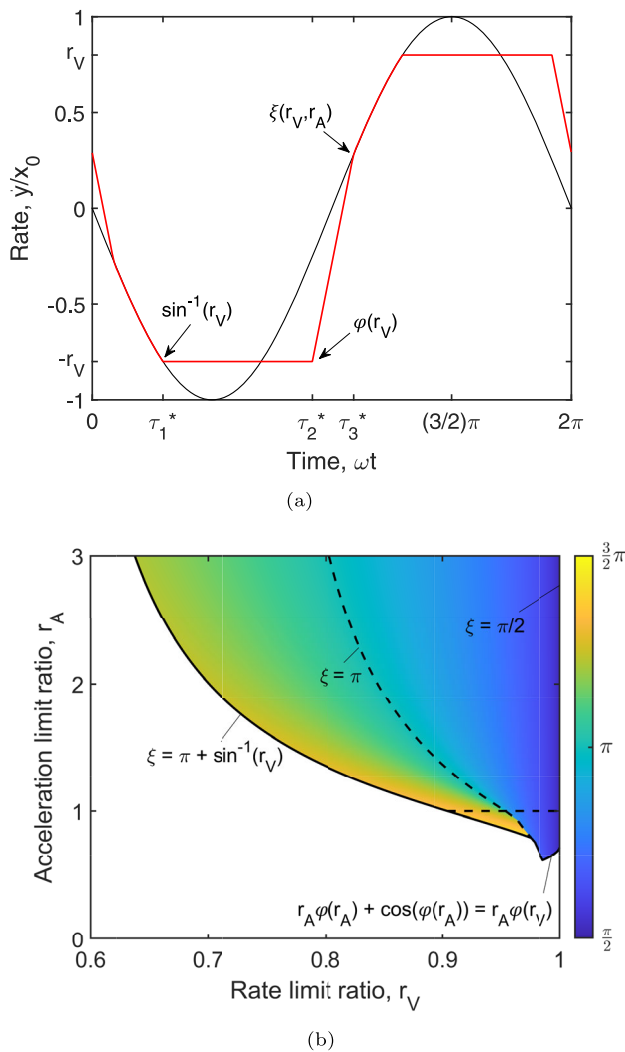


Fig. 6 (a) Steady-state output rate of a rate- and acceleration-limited actuator under sinusoidal input for $r_V = 0.8$ and $r_A = 2$ and (b) evolution of the non-dimensional ending time of the acceleration saturation interval in mixed partial saturation regime

2.3.2 Partial rate saturation with acceleration limit $r_A \geq 1$

The saturation regime scenario is more complex for those signals whose rate limit ratio is included in the range between r^* and 1. In this case, the acceleration limit can affect the actuator output in two different ways: for $r_A \geq 1$, its effect is still limited to the saturation of the acceleration peaks generated by the discontinuities in the output rate; differently, for $r_A < 1$, acceleration saturation also occurs in the sinusoidal (unsaturated) traits of the steady-state response. The first case is dealt with in this subsection, while the second case will be discussed in subsection 2.3.3.

An example of the effect of the combined rate and acceleration limit for $r^* < r_V < 1$ and $r_A \geq 1$ is provided in Fig. 6a, where the actuator output rate is shown for $r_V = 0.8$ and $r_A = 2$. It is possible to observe how the acceleration limit

is activated by the discontinuity generated by the rate limit at $\tau_2^* = \varphi(r_V)$, leading to an acceleration saturation (shown by the linear variation of the rate) between this point and the subsequent intersection with the sinusoidal input. Let us denote the non-dimensional ending time of the acceleration saturation as ξ , which is defined by the implicit equation

$$r_A(\xi - \varphi(r_V)) + \sin \xi = r_V. \quad (20)$$

Equation (20) has been solved numerically for varying r_V and r_A , within the parameter space region where mixed partial saturation occurs, as delimited by the boundaries derived in the remainder of this section. Solutions were computed using the Matlab function `fzero`, searching for roots within the interval $\xi \in [\pi/2, \pi + \sin^{-1}(r^*)]$. The resulting evolution of ξ with r_V and r_A is graphically represented in Fig. 6b. Limiting the present discussion to the case $r_A \geq 1$, it is possible to observe the minimum value of ξ is $\pi/2$ when $r_V = 1$, i.e., when no rate saturation occurs, while $\xi \rightarrow \varphi(r_V)$ when $r_A \rightarrow \infty$. In general, ξ monotonically increases for decreasing rate limit ratios (due to the increase of $\varphi(r_V)$) and for decreasing acceleration limit ratios, due to the increased duration of the acceleration saturation interval.

The saturation regime of the above signal can be referred to as *mixed partial saturation*, since it involves both rate and acceleration saturation while leaving part of the sinusoidal signal not saturated. The output position, rate and acceleration of the case $r_V = 0.8$ and $r_A = 2$ are represented in Fig. 7a. As the rate limit ratio is further decreased, a transition to full mixed saturation regime (Fig. 7b) is observed when the acceleration saturation covers the whole interval between the end of the first rate saturation and the start of the subsequent rate saturation, i.e., when $\xi = \pi + \sin^{-1}(r_V)$. By substituting this value into Eq.(20), it results that the boundary between full and partial mixed saturation regimes can be written, for $r_A \geq 1$, as

$$r_A = \frac{2r_V}{\pi + \sin^{-1}(r_V) - \varphi(r_V)}. \quad (21)$$

For $r^* < r_V < 1$, the phase delay introduced by rate and acceleration limits in mixed full saturation regime can be evaluated as

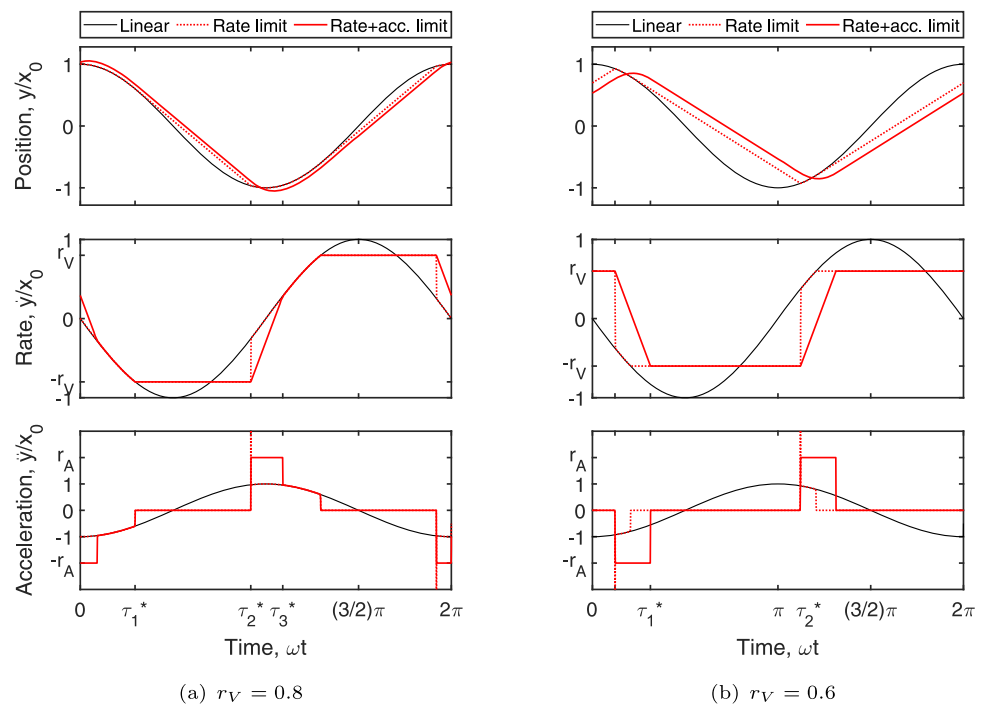
$$\Delta\tau = \varphi(r_V) + \frac{r_V}{r_A} - \pi, \quad (22)$$

therefore differing from that provided by Eq.(17) for $r_V < r^*$.

2.3.3 Partial rate saturation with acceleration limit $r_A < 1$

In the region of the parameter space characterised by $r^* < r_V < 1$ and $r_A < 1$, the acceleration limit can saturate not

Fig. 7 Steady-state response of a rate- and acceleration-limited actuator to sinusoidal input for $r_A = 2$



only the spikes generated by discontinuities in the output rate, but also the sinusoidal traits of the signal, leading to a complex combination of possible saturation regimes. In general, it can be stated that:

- saturation of acceleration peaks generated by rate discontinuities occurs between $\tau = \varphi(r_V)$ and $\tau = \xi$;
- saturation of the sinusoidal trait (i.e., not rate saturated) of the output signal occurs between $\tau = \cos^{-1}(r_A)$ and $\tau = \varphi(r_A) + \pi/2$, as shown in subsection 2.2.

In the context of mixed partial saturation, this can lead to two different actuator responses. From Fig. 6b, it can be observed that, when $r_A < 1$, a jump discontinuity occurs across the line $\xi = \pi$. In particular, it is found that, moving across such a line (in the direction of increasing r_V), the value of ξ has a sharp drop from $\varphi(r_A) + \pi/2$ to $\cos^{-1}(r_A)$. Therefore, when $\xi > \pi$, the sine saturation time interval is fully included in the peak saturation interval, so that only the latter is observed, as shown in Fig. 8a. Differently, when $\xi < \pi$, two distinct acceleration saturation intervals are observed, as indicated in Fig. 8b.

The regime transition from mixed partial saturation with $\xi > \pi$ to mixed full saturation occurs across the boundary indicated by Eq.(21), as already discussed for $r_A \geq 1$. The remaining regime transitions are represented in Fig. 9a and discussed in what follows.

- The transition from mixed partial saturation with $\xi < \pi$ to full mixed saturation simply occurs across the line $\xi = \pi$, after this intersects with the boundary from Eq.(21).
- For $r_A \leq r^\wedge$, mixed partial saturation ($\xi < \pi$) can also transition to a partly saturated acceleration regime. This transition occurs when the rate limit value is no longer reached in the rate output (see the case $r_V = 0.99$ in Fig. 9b). The boundary can be implicitly formulated as

$$r_A \left(\varphi(r_A) - \varphi(r_V) + \frac{\pi}{2} \right) + \cos(\varphi(r_A)) = r_V. \quad (23)$$

- Also for $r_V < 1$, the final transition from partial to full acceleration saturation occurs at $r_A = r^*$. However, transitions can also take place for larger values of r_A , as graphically explained in Fig. 9b. Let us consider the case $r_V = 0.97$. As r_A is progressively decreased, the saturation regimes transition first to mixed full saturation across the boundary $\xi = \pi$, then to full acceleration saturation across the boundary from Eq.(18). A further transition to partly saturated acceleration occurs when the linear trait of the saturated output is such to intersect the sinusoidal input. The boundary corresponding to this regime transition can be implicitly expressed as

$$r_A (\varphi(r_A) - \varphi(r_V)) + \cos(\varphi(r_A)) = 0. \quad (24)$$

Due to their implicit nature, the evaluation of the boundaries in Eqs.(23) and (24) is carried out numerically by assigning r_V as an input parameter and computing the corresponding boundary value of r_A using the Matlab function `fzero`.

Fig. 8 Steady-state response of a rate- and acceleration-limited actuator to sinusoidal input for $r_A = 0.9$

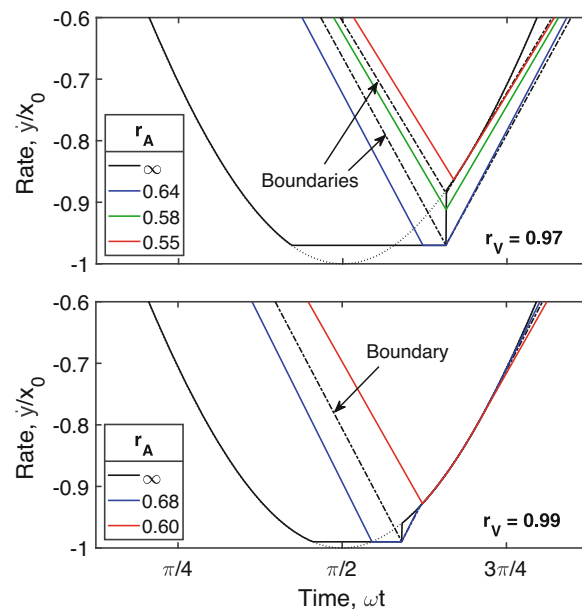
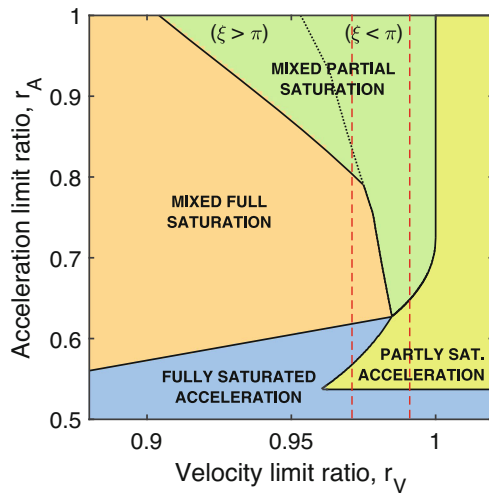
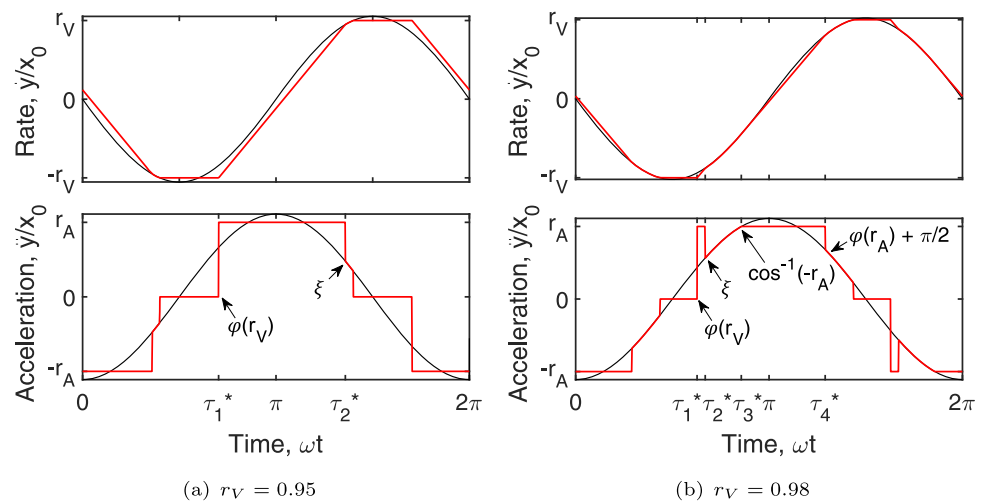


Fig. 9 (a) Detail of the saturation regimes in the parameter space $r_V - r_A$ and (b) steady-state output rate for varying acceleration limit ratio at $r_V = 0.97$ and $r_V = 0.99$

While the full acceleration saturation regime has already been characterised in subsection 2.2, it has also been shown that the phase delay can assume different values depending on the considered region in the parameter space $r_V - r_A$. For $r^* < r_V < 1$, two different behaviours are possible, as shown in Fig. 9b:

- if the switch between the positive and negative saturated traits occurs across the sinusoidal input, the presence of a rate limit is irrelevant and the phase delay will be equal to $\cos^{-1}(r_A)$, as in the absence of rate limit;
- if the switch occurs at the discontinuity generated by the rate limit at $\tau = \varphi(r_V)$, the phase delay will be $\varphi(r_V) - \pi/2$.

The boundary between these two behaviours, shown in Fig. 9b by means of a dashed black line, can be formulated as

$$r_A = \frac{2}{\pi} \sin(\varphi(r_V)). \quad (25)$$

2.4 Saturation regimes overview

In Fig. 10, the boundaries among the saturation regimes, derived in previous subsections, are graphically represented

$$r_V - r_A$$


$r^* \leq r_A \leq r^\wedge$, where several saturation regimes can take place as a result of small variations in r_V or r_A .

functions

In this section, sinusoidal describing functions are analytically derived for rate- and acceleration-limited systems, for each of the saturation regimes characterised in the previous section. Describing functions can be defined as the ratio between the fundamental harmonic component (first term of the Fourier series) of output and input signals. These functions can be used as a nonlinear extension of the linear concept of transfer function to analyse the behaviour of nonlinear systems that effectively act as low-pass filters [19], such as those including rate and/or acceleration limits. In fact, even when non-sinusoidal inputs are considered, these systems can effectively suppress higher harmonics, rendering the approximation introduced with the use of quasi-linear

describing functions acceptable. The describing function of the rate limit, already introduced in several publications (see, e.g., [10, 20, 25]), will be derived in subsection 3.1 to support the following discussion. The describing functions of the acceleration limit and of combined rate and acceleration limits, whose analytical formulations have not been previously derived to the best of the authors' knowledge, will be introduced in subsections 3.2 and 3.3, respectively.

3.1 Rate limit

In order to derive the describing function N_V of the rate limit, let us first determine in which frequency range this nonlinearity is active. Based on Eq.(3), it can be deduced that the actuator's response will be unaffected by the presence of the rate limit for angular frequencies smaller than or equal to

$$\omega_V = \frac{R_V}{x_0}, \quad (26)$$

where ω_V will be referred to as the rate limit *onset frequency*, and represents the value of ω such that $r_V = 1$. Similarly, the transition from partial to full saturation will take place at higher frequencies when $r_V = r^*$, i.e., when

$$\frac{\omega^*}{\omega_V} = \frac{1}{r^*} \cong 1.862, \quad (27)$$

as also discussed in [9, 10]. In summary, no saturation occurs for $\omega \leq \omega_V$, partial rate saturation occurs for $\omega_V < \omega < \omega_V/r^*$ and full rate saturation occurs for $\omega \geq \omega_V/r^*$.

Let us now determine the analytical expression of the rate limit describing function in these three frequency ranges. While the describing function is trivially equal to unity for $\omega \leq \omega_V$, the analytical formulation in full rate saturation

regime can be determined as the ratio between the main harmonic components of the triangle wave response introduced in Sect. 2.1 and of the sinusoidal input. Considering the triangle wave amplitude, equal to $(\pi/2)r_V$ under unitary sinusoidal input, and the phase delay provided by Eq.(12), the describing function can be expressed as

$$N_V(r_V) = \frac{4}{\pi} r_V e^{-j \cos^{-1}(\frac{\pi}{2} r_V)}. \quad (28)$$

It is worth noting that the above expression of the describing function only depends on the rate limit ratio (or on the ratio ω/ω_V if the equation is expressed in terms of the angular frequency). An analytical expression can also be similarly derived in partial saturation regime, although cubic spline interpolation is often used to reconstruct the function N_V in the corresponding frequency range (see, e.g., [10, 20]). The formulation derived by Roman and Ponce in [25] for partial saturation regime, rewritten according to the notation proposed in this paper, reads as

$$\begin{aligned} \operatorname{Re}\{N_V(r_V)\} = & \frac{1}{\pi} \left\{ \pi + \sin^{-1}(r_V) - \varphi(r_V) \right. \\ & \left. + r_V \sqrt{1 - r_V^2} + \frac{1}{2} \sin(2\varphi(r_V)) - 2r_V \cos(\varphi(r_V)) \right\} \end{aligned} \quad (29)$$

$$\operatorname{Im}\{N_V(r_V)\} = \frac{1}{\pi} [r_V - \sin(\varphi(r_V))]^2. \quad (30)$$

The resulting describing function, accounting for full, partial and no saturation regimes, is represented in Fig. 11. Gain and phase angle of N_V are plotted as functions of the normalised frequency ω/ω_V , therefore holding for any value of the rate limit R_V and of input amplitude x_0 . It can be observed that, after a gradual decrease occurring in the partial rate saturation frequency range, the gain is reduced at -20 dB/decade in full rate saturation, thus confirming the low-pass filter behaviour of the rate limit.

3.2 Acceleration limit

The describing function of the acceleration limit can be determined with the same procedure described above for the rate limit. Let us first introduce the onset frequency of the acceleration limit as

$$\omega_A = \sqrt{\frac{R_A}{x_0}}, \quad (31)$$

so that $\omega = \omega_A$ when $r_A = 1$ and, consequently, $r_A = (\omega_A/\omega)^2$. The derivation of the describing function N_A can be simplified by noting that the effect of the acceleration limit on the steady-state output rate, shown in Fig. 3, is the same as the rate limit effect on the actuator output position (Fig.

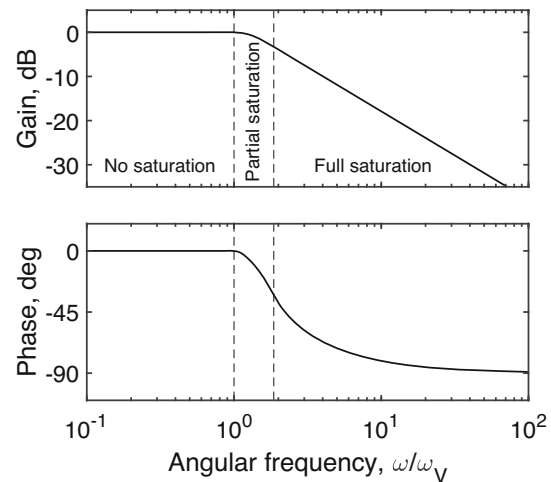


Fig. 11 Bode plot of the describing function N_V of the rate limit non-linearity

1), with the only addition of a phase lead equal to $\pi/2$. This implies that

$$jN_A(r_A) = e^{j\frac{\pi}{2}} N_V(r_V), \quad (32)$$

and, therefore,

$$N_A(r_A) = N_V(r_V). \quad (33)$$

It can be concluded that N_A has the same analytical expression as N_V (see Eqs.(28)-(30)) by simply replacing r_A to r_V . As a result, the behaviour of the acceleration limit describing function, represented in Fig. 12, is very similar to that described for N_V , with two following main differences. First, the Bode plot reveals that the gain is reduced at -40 dB/decade in full acceleration saturation regime, as opposed to the -20 dB/decade slope observed when full rate saturation occurs. In fact, due to the dependence of r_A on ω^2 , the acceleration limit has a stronger effect on the actuator output at high frequencies compared to the rate limit. In the same figure, the phase angle is also decreased with a higher rate by the acceleration limit; however, both rate and acceleration limits lead to a phase angle of -90 degrees for $\omega \rightarrow \infty$.

3.3 Combined rate and acceleration limit

In this subsection, analytical formulations for the describing function N_{VA} of combined rate and acceleration limits are derived based on the findings presented in Sect.2.3. When $r_V \geq 1$, the output signal is not affected by the rate limit, and therefore the formulations provided in Eqs.(28)-(30) can be directly used for full and partial acceleration saturation regimes, after the position in Eq.(33) is applied. For partial acceleration saturation, the same formulations can also be

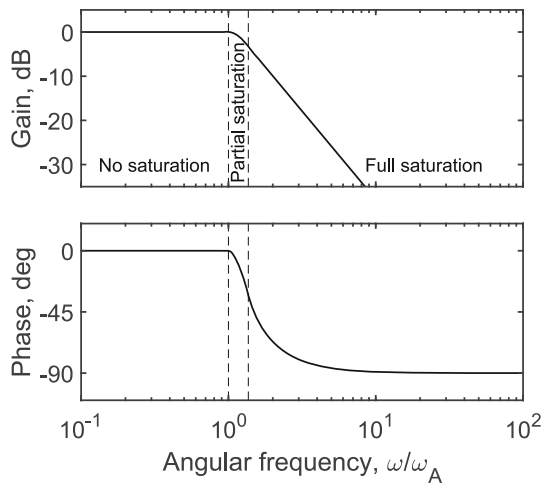


Fig. 12 Bode plot of the describing function N_A of the acceleration limit nonlinearity

used in the small parameter space region where this regime takes place for $r_V < 1$, where the steady-state response is unaffected by the rate limit. For the remaining saturation regimes, analytical formulations of the describing function are provided in what follows for $r_V < 1$.

3.3.1 Full acceleration saturation regime

Based on the results discussed in Sect. 2.3, it can be stated that, in full acceleration saturation regime, the steady-state response is a triangle wave of amplitude $(\pi/2)r_A$, regardless of the rate limit value. The amplitude of the describing function can therefore be determined by Eqs. (28) and (33) as

$$|N_{VA}| = \frac{4}{\pi} r_A. \quad (34)$$

The phase angle of the describing function, due to the symmetry of the steady-state response in this saturation regime, coincides with the phase delay between input and output maxima, for which expressions have been provided throughout Sect. 2, leading to

$$\angle N_{VA} = \begin{cases} \cos^{-1}\left(\frac{\pi}{2}r_A\right), & \text{if } r_A \leq \frac{2}{\pi} \sin(\varphi(r_V)) \\ \varphi(r_V) - \frac{\pi}{2}, & \text{if } r^* < r_V < 1 \cap r_A > \frac{2}{\pi} \sin(\varphi(r_V)) \\ \frac{\pi}{2} + \cos^{-1}\left(\frac{\pi}{2}r_V\right), & \text{if } r_V \leq r^* \end{cases} \quad (35)$$

3.3.2 Mixed full saturation regime

In mixed full saturation regime, the actuator output rate is a trapezoidal wave of amplitude r_V and linear traits with rate equal to $\pm r_A$, as shown in Fig. 5. The amplitude of the

describing function can therefore be easily derived as

$$|N_{VA}| = \frac{4}{\pi} r_A \sin\left(\frac{r_V}{r_A}\right). \quad (36)$$

The symmetry of the steady-state response allows, also in this case, for the evaluation of describing function phase as the phase delay provided in Sect. 3.1. From Eqs. (17) and (22), it is possible to write

$$\angle N_{VA} = \begin{cases} \varphi(r_V) + \frac{r_V}{r_A} - \pi & \text{if } r^* < r_V < 1 \\ \frac{r_V}{r_A} + \cos^{-1}\left(\frac{\pi}{2}r_V\right) & \text{if } r_V \leq r^*. \end{cases} \quad (37)$$

It is worthwhile underlining that the above equations reduce to Eqs. (34) and (35) for $r_V/r_A = \pi/2$, i.e., in correspondence of the boundary expressed by Eq. (18), warranting continuity between mixed and acceleration-only full saturation regimes.

3.3.3 Mixed partial saturation regime

The procedure for evaluating the describing function N_{VA} in mixed partial saturation regime cannot be simplified as in fully saturated regimes, not only due to the complex patterns of the actuator output, but also due to the absence of any symmetries in the steady-state response besides antiperiodicity. Therefore, the derivation of the describing function can only be carried out through a full evaluation of the Fourier coefficients of the first harmonic component of the signal. However, the calculation can be notably simplified by referring to the actuator output acceleration (or rate) rather than the output position, as detailed in the following equation:

$$\begin{aligned} N_{VA} &= \frac{2}{\pi x_0} \int_{t_1^*}^{t_1^* + \pi} y(t) e^{j\omega t} dt \\ &= -\frac{2}{\pi \omega^2 x_0} \int_{t_1^*}^{t_1^* + \pi} \ddot{y}(t) e^{j\omega t} dt \\ &= -\frac{2}{\pi} \int_{\tau_1^*}^{\tau_1^* + \pi} \ddot{y}''(\tau) e^{j\tau} d\tau. \end{aligned} \quad (38)$$

In the above formulation, the integration is carried out over the half period included between $\tau_1^* = \sin^{-1}(r_V)$ (the starting point of the rate saturation) and $\tau_1^* + \pi$ rather than over the interval $[0, \pi]$ for mathematical convenience. In the parameter space regions where, within mixed partial saturation regime, the acceleration limit only leads to the saturation of the acceleration peaks generated by rate discontinuities (i.e., for $\xi \geq \pi$ and for $\xi < \pi$ with $r_A \geq 1$), Eq. (38) reduces

to

$$N_{VA} = -\frac{2}{\pi} \left[\int_{\varphi(r_V)}^{\xi} r_A e^{j\tau} d\tau - \int_{\xi}^{\tau_1^* + \pi} \cos(\tau) e^{j\tau} d\tau \right] \quad (39)$$

and yields

$$\begin{aligned} \operatorname{Re}\{N_{VA}\} &= \frac{1}{\pi} \left\{ \pi + \sin^{-1}(r_V) - \xi \right. \\ &\quad \left. + r_V \sqrt{1 - r_V^2} - \frac{1}{2} \sin(2\xi) \right. \\ &\quad \left. - 2r_A [\sin \xi - \sin(\varphi(r_V))] \right\} \end{aligned} \quad (40)$$

$$\begin{aligned} \operatorname{Im}\{N_{VA}\} &= \frac{1}{\pi} \left\{ r_V^2 - \sin^2 \xi + 2r_A [\cos \xi - \cos(\varphi(r_V))] \right\} \end{aligned} \quad (41)$$

Differently, when the acceleration limit also leads to the saturation of the sinusoidal signal (i.e., for $\xi < \pi$ with $r_A < 1$), Eq.(38) leads to

$$\begin{aligned} N_{VA} &= -\frac{2}{\pi} \left[\int_{\varphi(r_V)}^{\xi} r_A e^{j\tau} d\tau \right. \\ &\quad \left. - \int_{\xi}^{\cos^{-1}(-r_A)} \cos(\tau) e^{j\tau} d\tau \right. \\ &\quad \left. + \int_{\cos^{-1}(-r_A)}^{\varphi(r_A) + \frac{\pi}{2}} r_A e^{j\tau} d\tau \right. \\ &\quad \left. - \int_{\varphi(r_A) + \frac{\pi}{2}}^{\tau_1^* + \pi} \cos(\tau) e^{j\tau} d\tau \right], \end{aligned} \quad (42)$$

from which

$$\begin{aligned} \operatorname{Re}\{N_{VA}\} &= \frac{1}{\pi} \left\{ \frac{\pi}{2} + \sin^{-1}(r_V) - \varphi(r_A) \right. \\ &\quad \left. + \cos^{-1}(r_A) - \xi + r_V \sqrt{1 - r_V^2} \right. \\ &\quad \left. + r_A \sqrt{1 - r_A^2} + \frac{1}{2} [\sin(2\varphi(r_A)) - \sin(2\xi)] \right. \\ &\quad \left. - 2r_A [\sin \xi - \sin(\varphi(r_V)) + \cos(\varphi(r_A))] \right\} \end{aligned} \quad (43)$$

$$\begin{aligned} \operatorname{Im}\{N_{VA}\} &= \frac{1}{\pi} \left\{ r_V^2 + r_A^2 - \sin^2 \xi + \sin^2(\varphi(r_A)) \right. \\ &\quad \left. + 2r_A [\cos \xi - \cos(\varphi(r_V)) - \sin(\varphi(r_A))] \right\}. \end{aligned} \quad (44)$$

3.4 Overview for varying rate and acceleration limit

The analytical formulations derived in this section for the describing function N_{VA} enable a full description of the dynamic behaviour of an actuator with combined rate and acceleration limits for varying input frequencies. Figure 13a represents the describing function as a function of the normalised angular frequency ω/ω_V (corresponding to the

inverse of r_V). To address the dynamic behaviour introduced by all possible combinations of the rate and acceleration limit values, the parameter η_{VA} is introduced through the relationship:

$$r_A = \frac{R_A x_0}{R_V^2} r_V^2 = \eta_{VA} r_V^2. \quad (45)$$

The describing function of the rate limit ($\eta_{VA} \rightarrow \infty$) is also included as a limit case. The parabolic curves described by the above equation, characterised by constant values of η_{VA} , are plotted in the parameter space $r_V - r_A$ in Fig. 13b, with arrows pointing towards the direction of increasing frequency. Figure 13b enables a better visualisation of the transitions between different saturation regimes, which are also indicated by markers in Fig. 13a. It can be observed that:

- if $\eta_{VA} \geq 1$, the onset of nonlinear behaviour is driven by the rate limit and occurs when $r_V = 1$. For $\omega > \omega_V$, the actuator will go through partial and full mixed saturation, and will eventually operate in full saturated acceleration regime as $\omega \rightarrow \infty$;
- if $0.646 < \eta_{VA} \leq 1$, the onset of the nonlinearity is driven by the acceleration limit, occurring at $r_A = 1$, while partial acceleration saturation occurs for $\omega_V < \omega < \omega_A$. Starting from $\omega = \omega_V$, the actuator behaviour will be the same as for $\eta_{VA} \geq 1$;
- if $\eta_{VA} \leq 0.646$, rate saturation can never occur, independently of the input frequency. After the nonlinearity activation at $\omega = \omega_A$, a transition from partial to full acceleration saturation will occur at $\omega = \omega_A/r^*$.

The Bode plot of the describing function (Fig. 13a) clearly shows the low-pass filter behaviour induced by the rate and acceleration limits. As discussed above, in the presence of a finite acceleration limit, full acceleration saturation regime always occurs for $\omega \rightarrow \infty$; therefore, a gain reduction of 40 dB/decade is observed at high frequencies for any η_{VA} . Actuators characterised by small values of η_{VA} behave very similarly to systems with acceleration limit only, while full and partial mixed saturation regimes occur in more and more extended frequency ranges as η_{VA} is increased, until the behaviour of a rate-limited system is asymptotically recovered.

The phase angle introduced by these combined actuator nonlinearities tends to -180 degrees for $\omega \rightarrow \infty$, for any value of η_{VA} , differently from the behaviour observed for systems with rate or acceleration limit only, where the asymptotic values at high frequencies is equal to -90 degrees. When the rate limit is the dominating nonlinearity ($\eta_{VA} > 1$), the phase angle gradually decreases for increasing frequency across the partial and full mixed saturation regimes. However,

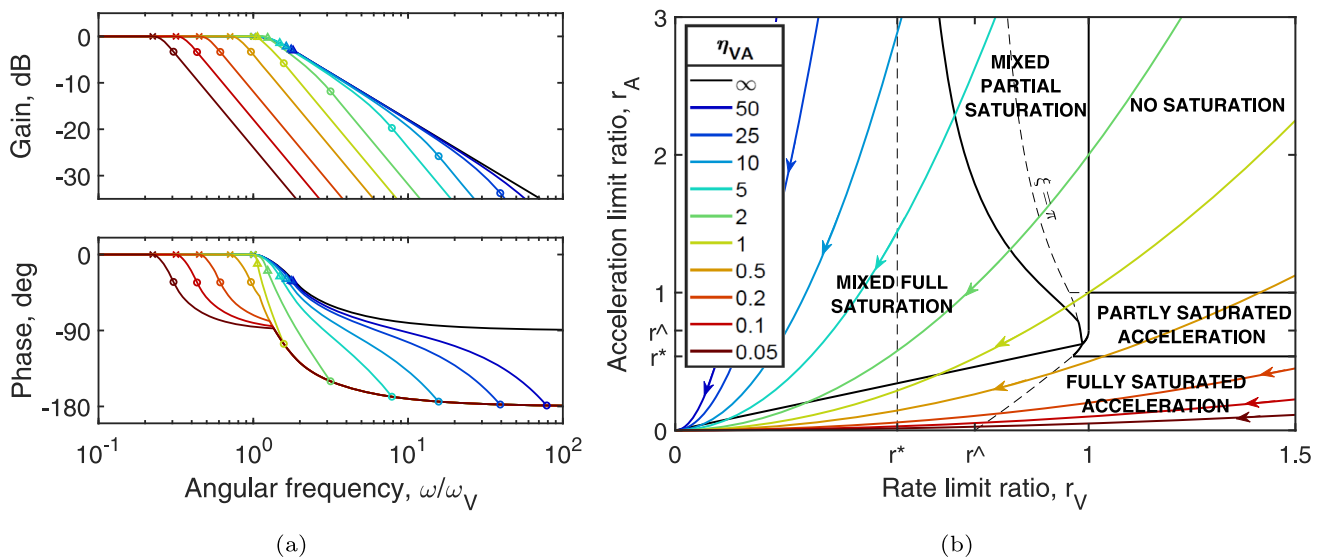


Fig. 13 Describing function of combined rate and acceleration limits for varying angular frequency and η_{VA} (a) and corresponding input curves in the parameter space $r_V - r_A$ (b). Cross markers: onset points; triangle markers: partial to full mixed saturation; circle markers: transitions to fully saturated acceleration

a sudden change in behaviour is observed when the transition from mixed to acceleration only full saturation regimes occurs; here, an angular point can be observed. In system dominated by the acceleration limit ($\eta_{VA} < 1$), the phase angle first gradually decreases towards -90 degrees across partial saturation regimes and even full acceleration saturation regime as long as $r_V > r^*$. However, when $r_V = r^*$, another nonsmooth change can be observed in this pattern. Following this angular point, all curves follow the same decreasing pattern towards the asymptotic -180 degrees value; in fact, as shown in Eq.(19), in this saturation regime the phase angle only depends on the rate limit ratio (or, equivalently, on the normalised frequency ω/ω_V). The described phase angle patterns emphasise that cubic spline interpolation, often considered for addressing the describing function in partial saturation regime for the rate limit nonlinearity, would lead to misleading results if used in the presence of rate and acceleration limits.

4 Analysis of closed-loop systems

One of the main purposes of describing functions is the analysis of closed-loop systems containing nonlinear elements. By replacing the nonlinearity with its quasi-linear approximation expressed by the describing function, it is possible to determine the presence of nonlinearity-induced limit cycle oscillations and investigate the effect of the nonlinearity on the system performance and stability. In this section, a describing function analysis is performed on a basic case-study, consisting of the closed-loop system illustrated in Fig.

14, which includes a first-order system governed by the transfer function

$$C(s) = \frac{K}{1 + Ts}, \quad (46)$$

where K is the system gain, T the time constant and s the Laplace variable, and a nonlinear element denoted by N , which will feature the describing functions derived for the rate limit and combined rate and acceleration limits nonlinearity. While the above system is only used in this paper as a case-study, a possible physical interpretation of this setup is to model separately the linear dynamics of the actuator, accounting for instance for its cut-off frequency and bandwidth, and its nonlinear elements; such models are often encountered in the literature (see, e.g., [10, 19]). Following the approach first introduced by Gilbreath [10] for rate-limited systems, and later applied by Yuan et al. to the analysis of first-order systems with time delay [20], a describing function analysis is here performed to achieve the identification of the onset frequency of the nonlinear behaviour, and the derivation of an equivalent describing function for the closed-loop system. In addition to adapting the proposed methodology to address both rate and acceleration limit nonlinearities, the technique is also extended to investigate the occurrence of jump resonances, which can be responsible for multiple stable solutions and unexpected dynamic behaviour.

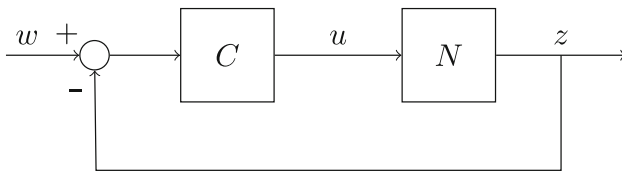


Fig. 14 First-order closed-loop system with a nonlinear element

4.1 Onset point of nonlinearity

In closed-loop systems, the onset point of the rate limit corresponds to the angular frequency $\tilde{\omega}_V$ for which the condition $r_V = 1$ is verified. Denoting with w_0 the amplitude of the input signal of the feedback loop, the closed-loop onset frequency can be evaluated from Eq.(4) as

$$w_0 \left| \frac{u}{w} (j\tilde{\omega}_V) \right| = \frac{R_V}{\tilde{\omega}_V}, \quad (47)$$

where u/w is the transfer function between u and w . The behaviour of the system at the onset point is still linear (i.e., $N(j\tilde{\omega}_V, u_0) = 1$), therefore Eq.(47) can be rewritten for the given system as

$$\tilde{\omega}_V \left| \frac{C(j\tilde{\omega}_V)}{1 + C(j\tilde{\omega}_V)} \right| = \frac{R_V}{w_0}. \quad (48)$$

Similarly, the closed-loop onset frequency of an acceleration-limited system can be evaluated by imposing the condition $r_A = 1$. From Eq.(14),

$$w_0 \left| \frac{u}{w} (j\tilde{\omega}_A) \right| = \frac{R_A}{\tilde{\omega}_A^2}. \quad (49)$$

If actuator rate and acceleration limits are both taken into account, the closed-loop onset frequency of the actuator nonlinearity will be the smallest value between $\tilde{\omega}_V$ and $\tilde{\omega}_A$, consistently with the findings presented in Sect. 3.4. It is worth mentioning that, in more complex systems, the above equations might admit multiple solutions, meaning that the system undergoes multiple transitions between linear and nonlinear behaviours. In the specific case of combined rate and acceleration limits, linear behaviour will only be observed in those intervals where simultaneously $r_V \geq 1$ and $r_A \geq 1$.

4.2 Equivalent describing function of the feedback loop

Deriving an equivalent describing function to approximate the nonlinear behaviour of the feedback loop offers two main advantages. Firstly, the closed-loop describing function provides a quasi-linear relationship between the input

and output of the feedback loop, which can be used to investigate the response of the system in the frequency domain, and even to replace the entire feedback loop in the context of larger systems, allowing for a quasi-linear investigation of the overall system. Secondly, the open-loop describing function provides an useful insight into the dynamic stability of the system, enabling the evaluation of the effect of the nonlinearity on the gain and phase margins.

The describing function of a basic closed-loop system, as that investigated in this section, is characterised by two main behaviours: below the closed-loop onset frequency, the system still behaves linearly; above this frequency, the system is affected by the rate and acceleration limits and exhibits a nonlinear behaviour, which will be characterised in the following discussion.

Let us write system input signal in the complex time domain as

$$w(t) = w_0 e^{j\omega t}. \quad (50)$$

Then, the input signal of the nonlinear element can be expressed as

$$u(t) = u_0 e^{j(\omega t + \phi)} = \frac{C(j\omega)}{1 + C(j\omega)N(j\omega, u_0)} w(t), \quad (51)$$

from which

$$u_0(j\omega, w_0) = \left| \frac{C(j\omega)}{1 + C(j\omega)N(j\omega, u_0)} \right| w_0. \quad (52)$$

Since the describing function value depends on the amplitude u_0 , Eq.(52) is an implicit nonlinear equation and, in this study, is solved numerically using a constrained nonlinear optimisation approach, implemented by the Matlab function `fmincon` [37].

Once u_0 is determined, the rate and acceleration limit ratios can be evaluated from Eqs.(4) and (14) respectively, and the describing function of the nonlinear element can be derived using the formulations proposed in Sect. 3. Finally, the closed-loop describing function N_{cl} of the feedback loop (i.e., between w and z) can be evaluated by using standard linear techniques as

$$N_{cl}(j\omega, w_0) = \frac{C(j\omega)N(j\omega, u_0)}{1 + C(j\omega)N(j\omega, u_0)}, \quad (53)$$

while the equivalent open-loop describing function can be obtained from the above expression as

$$\begin{aligned} N_{ol}(j\omega, w_0) &= \frac{N_{cl}(j\omega, w_0)}{1 - N_{cl}(j\omega, w_0)} \\ &= C(j\omega)N(j\omega, u_0) \end{aligned} \quad (54)$$

4.3 Application to first-order systems

The proposed procedure for the evaluation of the onset point of the nonlinearity and the equivalent describing function of the feedback loop is here applied to two first-order systems with time constant set to $T = 0.1$ in Eq.(46) and two different values of the gain $K = 1$ and $K = 10$. Both closed-loop systems are subjected to an input signal of amplitude $w_0 = 1$ deg.

4.3.1 Rate limit

Figure 15 illustrates the evolution of the onset frequency of nonlinear behaviour for varying rate limit between 0.5 and 200 deg/s. For both systems, it is possible to observe that the onset frequency increases almost linearly with the rate limit for small values of R_V , while rapidly increasing for larger rate limits, with a vertical asymptote achieved at 10 deg/s for $K = 1$ and 100 deg/s for $K = 10$. Such a behaviour can be explained by evaluating Eq.(48) for small and large rate limits. In fact, for small R_V , and consequently $\tilde{\omega}_V \ll 1$, Eq.(48) yields

$$\tilde{\omega}_V \cong \frac{1 + K}{K} \frac{R_V}{w_0}, \quad (55)$$

while for $\tilde{\omega}_V \rightarrow \infty$ it is obtained that

$$R_V \rightarrow \frac{K}{T} w_0. \quad (56)$$

Beyond the rate limit value expressed by Eq.(56), Eq.(48) has no solutions and the rate limit will not affect the response of the system at any frequency. It is worth mentioning that the specific patterns discussed above strongly depend on the order of the system investigated. If, for instance, a second-order system (or a more complex system behaving as such at high frequencies) would still have a maximum effective rate limit, but would not exhibit the vertical asymptotes shown in Fig. 15.

The solution for the input and output amplitudes of the nonlinear element and the corresponding open-loop equivalent describing function are reported in Fig. 16 for the two systems, setting the rate limit to 5 deg/s. In the case $K = 1$, the nonlinear onset occurs at 1.8461 Hz, while for $K = 10$ the onset occurs at 0.8809 Hz. In Fig. 16a, it is possible to observe how the rate limit onset causes an increase in the amplitude u_0 compared to the linear case, particularly significant in the case $K = 10$, where u_0 increases by an order of magnitude. This causes a drop in amplitude and phase in the equivalent describing function. In Fig. 16b, it can be seen that after such a drop the open-loop describing functions settle to the same amplitude, characterised by a decaying slope

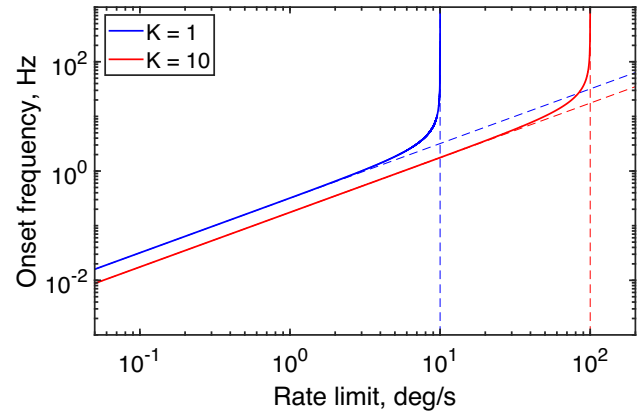


Fig. 15 Onset frequency for a rate-limited closed-loop first-order system ($w_0 = 1$ deg, $T = 0.1$ and varying R_V)

of -20 dB/decade. Observing from Fig. 16a that u_0 converges to its linear value at high frequencies, which can be approximated as

$$u_0 \cong \frac{K w_0}{\omega T}, \quad (57)$$

then it can be derived that, for $\omega \gg 1$, the gain of the open-loop describing function decay as

$$|N_{ol}| \cong \frac{4R_V}{\pi w_0 \omega}. \quad (58)$$

Similarly, it can be calculated that the output of the nonlinear element, which in this case coincides with the output of the system, is limited to

$$z_0 = \frac{4R_V}{\pi \omega} \quad (59)$$

when the system operates in full rate saturation regime. It is worth noting that the quantities evaluated by Eqs. (58) and (59) are completely independent of the system properties, depending only on the rate limit and input amplitude. However, the values of K and T affect the describing function phase, which for $\omega \rightarrow \infty$, tends to

$$\angle N_{ol} \cong \frac{\pi}{2} + \cos^{-1} \left(\frac{\pi}{2} \frac{T}{K} \frac{R_V}{w_0} \right). \quad (60)$$

A noteworthy phenomenon visible in Fig. 16 is that, in the case $K = 10$, the system undergoes a jump resonance, causing the existence of multiple solutions in a narrow frequency range closely located to the onset frequency of the rate limit. This phenomenon is discussed in detail in Sect. 4.4.

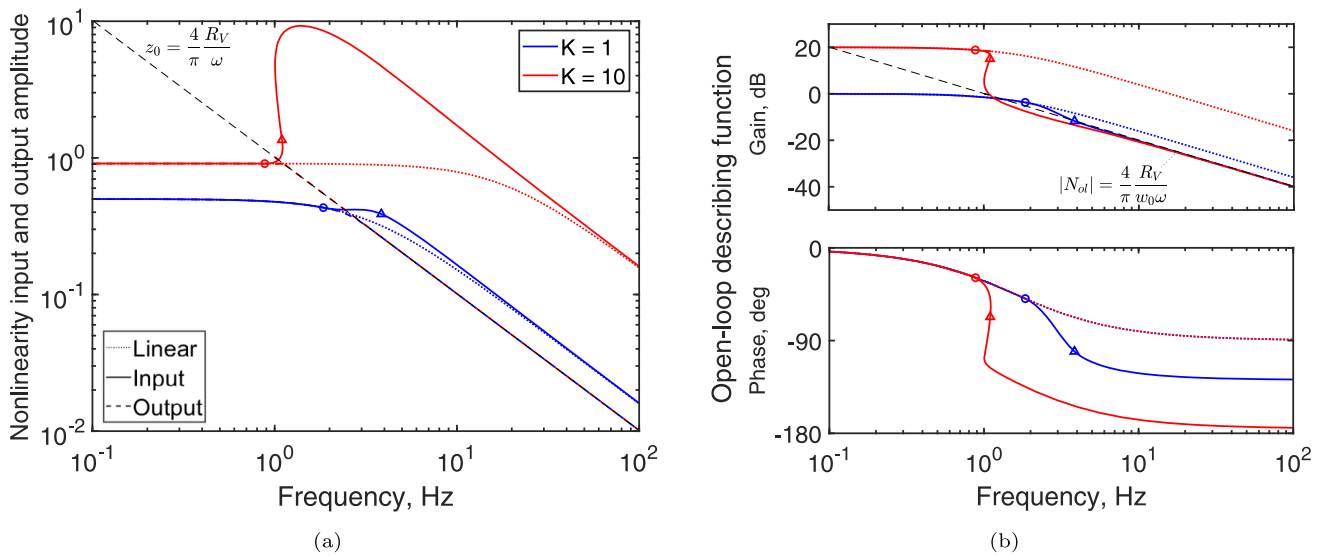


Fig. 16 Input and output of the nonlinearity (a) and open-loop describing function (b) for a rate-limited closed-loop first-order system ($R_V = 5$ deg/s, $w_0 = 1$ deg and varying K). Circle markers: rate limit onset; triangle markers: partial to full saturation

4.3.2 Combined rate and acceleration limits

Let us now focus on the case $K = 1$, imposing again a rate limit equal to 5 deg/s, along with a varying acceleration limit. The onset frequency is evaluated from Eqs.(47)-(49) and represented in Fig. 17. Bearing in mind that the onset frequency is the smallest value between $\tilde{\omega}_V$ and $\tilde{\omega}_A$, it is possible to see how the acceleration limit drives the onset for small values of R_A , where the onset frequency can be approximated as

$$\tilde{\omega}_A \cong \sqrt{\frac{1 + K}{K} \frac{R_A}{w_0}}, \quad (61)$$

shown by the dashed line in Fig. 17, while the rate limit prevails when the acceleration limit is larger than $R_A = R_V \tilde{\omega}_V = 53.59$ deg/s².

The input and output amplitudes of the nonlinear element and the open-loop equivalent describing functions are plotted in Fig. 18 for five values of the acceleration limit, ranging from 10 to 200 deg/s², while the rate limit is kept constant at 5 deg/s. Consistently with the result highlighted in Fig. 17, the nonlinear onset is only driven by the acceleration limit in the cases $R_A = 10, 20$ and 50 deg/s², while the rate limit drives the onset in the remaining cases. While the acceleration limit is generally responsible for a further increase in the nonlinearity input amplitude u_0 , the largest effect is observed for $R_A = 20$ deg/s², with a more moderate increase observed for $R_A = 10$ deg/s².

With respect to the high-frequency behaviour, u_0 is again approximated by Eq.(57), and it is therefore independent of the rate and acceleration limits, while the describing function

tends to

$$|N_{ol}| \cong \frac{4 R_A}{\pi w_0 \omega^2} \quad (62)$$

and the system output to

$$z_0 \cong \frac{4 R_A}{\pi \omega^2}. \quad (63)$$

Therefore, at high frequencies, N_{ol} and z_0 do not depend on the underlying linear system properties, as already established in the rate limit case, but only on the acceleration limit and input amplitude. Differently from the rate limit, the acceleration limit imposes a sharp amplitude decay, characterised by a -40 dB/decade slope. All describing function phase curves converge to the same value

$$\angle N_{ol} \cong \pi + \cos^{-1} \left(\frac{\pi}{2} \frac{T}{K} \frac{R_V}{w_0} \right). \quad (64)$$

Therefore, while the presence of rate limits is concealed by the stronger effect of the acceleration limits on the response amplitude at high frequencies, it is still possible to identify the rate limit value (if system properties are known) from the describing function phase, which is instead independent of the acceleration limit R_A .

It is noteworthy that jump resonance occurs for acceleration limits between 20 and 100 deg/s², but is not observed for either the largest or the smallest values investigated.

This behaviour can also be visualised in Fig. 19, where the input of the nonlinear element is plotted in the parameter space $r_V - r_A$, along with the boundaries of the saturation regimes. Jump resonance can be detected in this plot based on

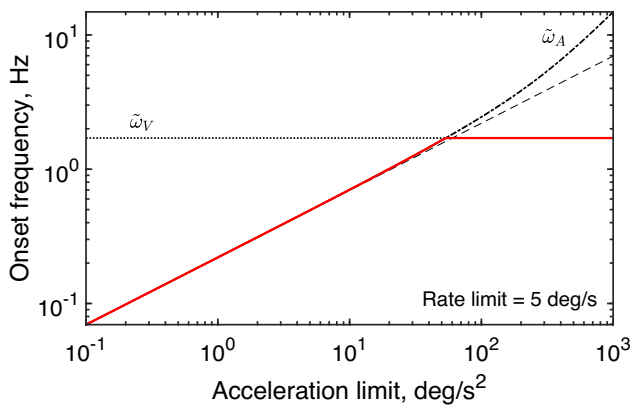


Fig. 17 Onset frequency for a rate- and acceleration-limited closed-loop first-order system ($w_0 = 1$ deg, $R_V = 5$ deg/s and varying R_A)

the following considerations. From the definitions of rate and acceleration limit ratios, from Eqs.(4) and (14) respectively, it can be deduced that

$$r_A = \frac{R_A}{R_V \omega} r_V. \quad (65)$$

If specific values of R_V and R_A are assigned, the above equation describes a pencil of lines through the origin, each one defined by a specific angular frequency value ω . If one of such lines intersects the nonlinearity input curve in more than one point, then multiple solutions are possible at that frequency, suggesting the presence of a jump resonance. In this case, the line characterised by the largest angular coefficient, corresponds to the supercritical fold bifurcation and, there-

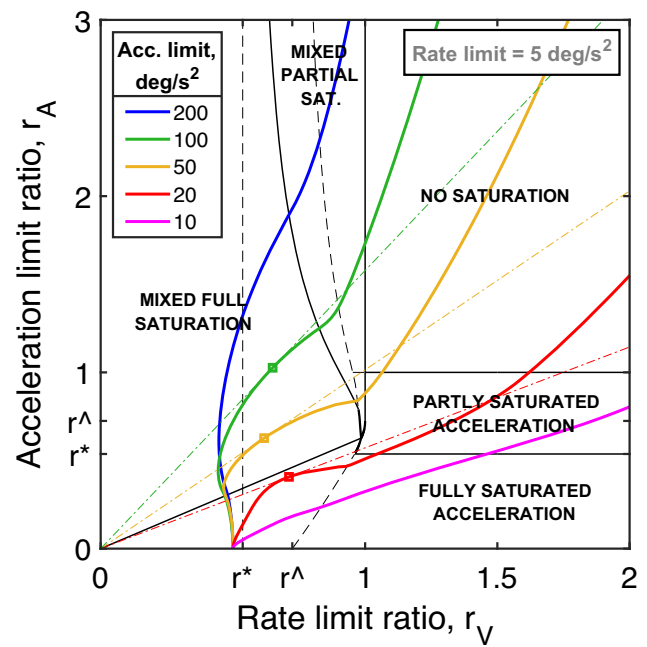


Fig. 19 Input curves of the nonlinearity in the parameter space $r_V - r_A$ for a rate- and acceleration-limited closed-loop first-order system ($w_0 = 1$ deg, $R_V = 5$ deg/s and varying R_A). The squared markers indicate the supercritical fold bifurcations, the dashed-dotted lines the bifurcation frequency

fore, to the lowest frequency where multiple solutions can occur. Such lines are plotted in Fig. 19 for the cases where jump resonance occurs, and the supercritical fold bifurcations are highlighted by square markers. The mathematical conditions for which jump resonance occurs across different saturation regimes are addressed in the following subsection.

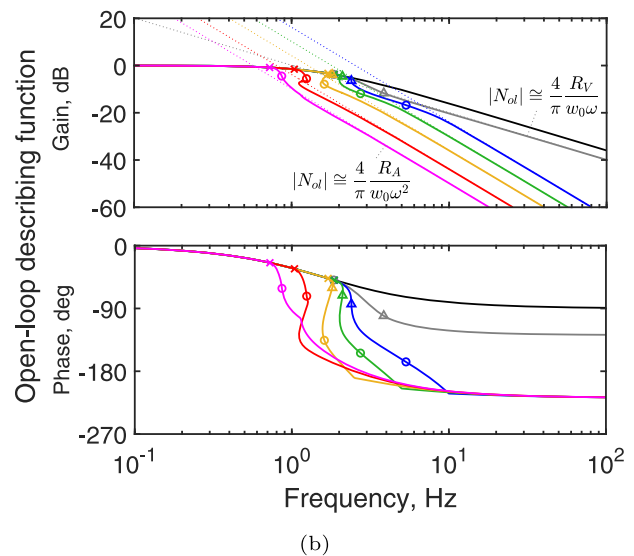
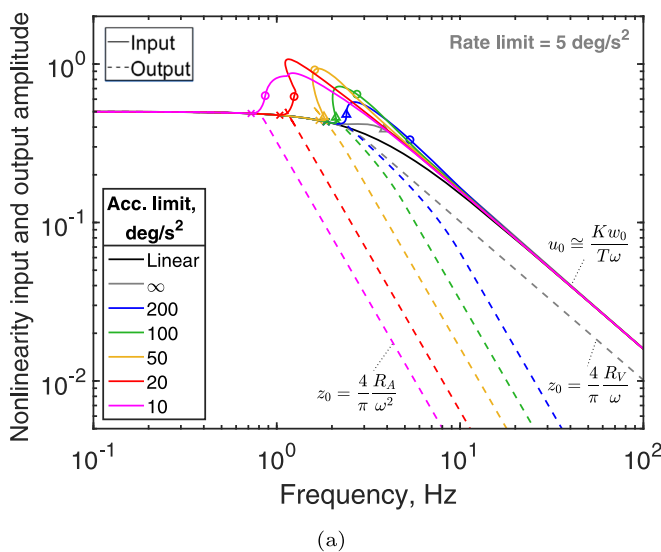


Fig. 18 Input and output of the nonlinearity (a) and open-loop describing function (b) for a rate- and acceleration-limited closed-loop first-order system ($R_V = 5$ deg/s, $w_0 = 1$ deg and varying R_A). Cross

markers: nonlinearity onset; triangle markers: partial to full mixed saturation; circle markers: transitions to full acceleration saturation

4.4 Jump resonance

The findings presented in the previous subsection highlight the possibility of jump resonance in the dynamic response of closed-loop systems with rate and/or acceleration limits, leading to the presence of multiple solutions at certain frequencies and, potentially, to sudden and unexpected variations in the frequency response (i.e., jumps between different solution branches), which can undermine the stability and degrade the performance of the system, as observed by Gilbreath [10] for rate-limited systems. In this subsection, the conditions for the occurrence of jump resonance in feedback loops with rate or combined rate and acceleration limits are derived, along with the supercritical fold frequency in the jump resonance, i.e. the lowest frequency where multiple solutions appear.

4.4.1 Rate limit

Let us consider the rate-limited system characterised by $K = 10$, investigated in the previous subsection. By replacing Eq.(28) into Eq.(52), it is possible to derive the closed-form solution for u_0 in full rate saturation regime as

$$u_0 = \sqrt{\left(\frac{a_1^2}{2} - a_2\right) \pm \frac{a_1}{2} \sqrt{a_1^2 - 4 \left[a_2 + \left(\frac{\pi R_V}{2\omega}\right)^2\right]}}, \quad (66)$$

where

$$\begin{cases} a_1 = \frac{8}{\pi} \operatorname{Im}\{C\} \cdot \frac{R_V}{\omega} \\ a_2 = 4 \left(\operatorname{Re}\{C\} + \frac{4}{\pi^2} |C|^2 \right) \left(\frac{R_V}{\omega} \right)^2 - (|C|w_0)^2. \end{cases} \quad (67)$$

The positive and negative branches of this solution are shown in Fig. 20. It is possible to observe that the supercritical fold of the complete solution to Eq.(52) coincides with the point where these two real solutions to Eq.(66) originate. The corresponding bifurcation frequency can therefore be determined by setting the inner radicand of Eq.(66) to zero. After the required algebraic steps, this results in

$$\omega_b = \frac{\pi R_V}{2|C(j\omega_b)|w_0} \left| 1 + \frac{8}{\pi^2} \operatorname{Re}\{C(j\omega_b)\} \right|. \quad (68)$$

If applied to the case $K = 10$ of the previous subsection, Eq.(68) yields $f_b = 1.0051$ Hz, in agreement with the behaviour shown in Fig. 16. However, as observed in the case $K = 1$, jump resonance does not always occur in the frequency response of rate-limited closed-loop systems. Since the above solution refers to full saturation regime, it

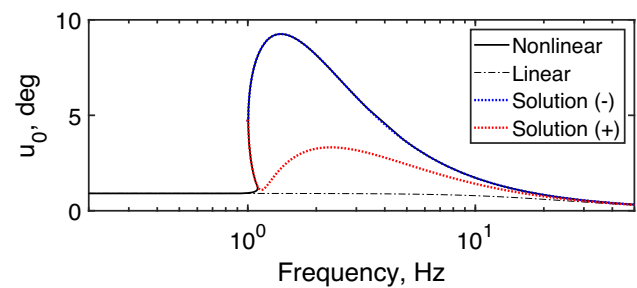


Fig. 20 Nonlinear input amplitude evolution with frequency for a rate-limited first-order closed-loop system ($R_V = 5$, $K = 10$, $T = 0.1$)

is required for its validity that $r_V \leq r^*$ for $\omega = \omega_b$. By replacing Eqs.(66) and (68) into Eq.(4), it can be derived that the condition for a rate-limited system to encounter jump resonance is

$$\operatorname{Im}\{C(j\omega_b)\} > \frac{\pi}{4}. \quad (69)$$

In the case of the first-order system investigated in this section, this condition cannot be satisfied for any rate limit if

$$K < \frac{\pi}{2}, \quad (70)$$

explaining the absence of bifurcations in the case $K = 1$.

Figure 21 shows the variation of the supercritical fold frequency with the rate limit for the case $K = 10$. The evolution of ω_b , obtained from Eq.(68), is quasi-linear for strict rate limits, where

$$\omega_b \cong \frac{\pi}{2Kw_0} \left(1 + \frac{8}{\pi^2} K \right) R_V, \quad (71)$$

and tends to a vertical asymptote for

$$R_V \rightarrow \frac{2}{\pi} \frac{K}{T} w_0. \quad (72)$$

Despite the domain of validity of this solution being restricted by Eq.(69) (see continuous line in Fig. 21), jump resonance occurs for a wide range of rate limits. In particular, starting from $R_V \cong 9.53$ deg/s, multiple solutions will appear in the dynamic response of the system at a lower frequency than the rate limit onset point. This implies that transition to latent nonlinear branches of the solution can occur even when the system is operating in linear regime.

4.4.2 Combined rate and acceleration limits

Let us now consider the case of a closed-loop system where rate and acceleration limits are applied, aiming to determine the conditions for the presence of jump resonance in the

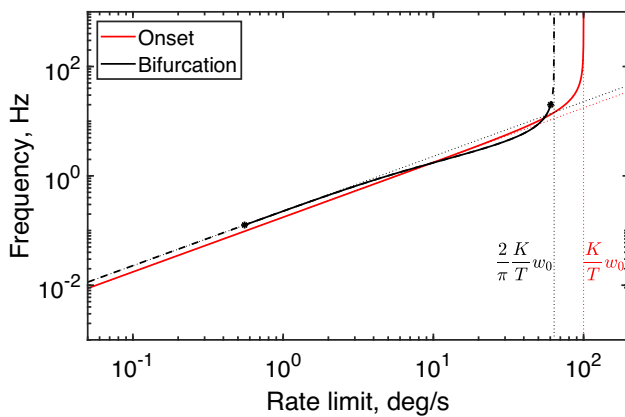


Fig. 21 Bifurcation frequency of a first-order closed-loop system ($K = 10$, $T = 0.1$) for varying rate limit

dynamic response and the value of the supercritical fold frequency, starting from which multiple solutions occur. In this case, the bifurcation analysis is notably complicated by the presence of several different saturation regimes. In the rate limit-only case, the supercritical fold of the dynamic response coincides with the point where two real solutions to Eq.(52) appear for the full rate saturation regime. From Fig. 19, it is clear that fold bifurcations in closed-loop systems with rate and acceleration limits can be associated with the existence of multiple analytical solutions to Eq.(52) in any full saturation regime. This includes acceleration and mixed full saturation regimes, each of them characterised by either $r_V \leq r^*$ or $r^* < r_V < 1$. These four cases will be discussed in what follows.

To determine the bifurcation frequency in full acceleration saturation when $r_V \leq r^*$, let us substitute the describing function expressed by Eqs.(34) and (35c) into Eq.(52). A closed-form solution for the dynamic response can be derived in the same form as Eq.(66), setting the coefficients a_1 and a_2 to

$$\begin{cases} a_1 = \frac{8}{\pi} \operatorname{Re}\{C\} \cdot \frac{R_A}{\omega^2} \\ a_2 = 4 \left(\operatorname{Im}\{C\} \cdot \frac{R_V}{\omega} + \frac{4}{\pi^2} |C|^2 \cdot \frac{R_A}{\omega^2} \right) \cdot \frac{R_A}{\omega^2} - (|C|w_0)^2. \end{cases} \quad (73)$$

Also in this case, the bifurcation frequency can be obtained by setting the radicand in Eq.(66) to zero, which results in

$$\omega_b = \frac{\pi R_V}{4|C(j\omega_b)|w_0} \cdot \left[1 + \sqrt{1 + \frac{64}{\pi^3} \frac{R_A}{R_V^2} |C(j\omega_b)|^2 \sin(\angle C(j\omega_b)) w_0} \right]. \quad (74)$$

The above solution only holds if the corresponding rate and acceleration limit ratios respect the boundary conditions of

the investigated saturation regime, which are expressed by $r_V \leq r^*$ and $r_V/r_A \geq \pi/2$, from Eq.(18). The value of u_0 corresponding to the supercritical fold point can easily be evaluated by Eq.(66), setting once again the radicand to zero and replacing the result of Eq.(74). Finally, the bifurcation frequency and corresponding value of u_0 can be used to determine r_V and r_A and verify whether the solution lies within the domain of validity defined by the aforementioned boundary conditions.

In full mixed saturation regime, if $r_V \leq r^*$, the solution can be determined by using the same procedure, considering the describing function defined by Eqs.(36) and (37b). This results in the bifurcation frequency

$$\omega_b = \frac{\pi R_V}{4|C(j\omega_b)|w_0} \cdot \left[1 + \sqrt{1 + \frac{64}{\pi^3} \frac{R_A}{R_V^2} \sin\left(\frac{R_V}{R_A} \omega_b\right)} \right] \cdot \sqrt{|C(j\omega_b)|^2 \cos\left(\angle C(j\omega_b) - \frac{R_V}{R_A} \omega_b\right) w_0}. \quad (75)$$

After evaluating ω_b , it can be verified whether the solution falls within the domain of validity defined by the boundaries $r_V \leq r^*$ and $r_V/r_A < \pi/2$, from Eq.(18), following the same procedure described above for the full acceleration saturation case.

The determination of the bifurcation frequency for $r^* < r_V < 1$ is notably complicated by the presence of the term $\varphi(r_V)$ in the describing function formulations, which does not allow for the separation of the variables u_0 and ω in the equations. Let us first consider the case of full acceleration saturation. Substituting Eqs.(34) and (35b), it is possible to rewrite Eq.(52) as

$$\begin{aligned} & u_0^2 + 2|C| \left(\frac{4R_A}{\pi\omega^2} \right) \cdot [\cos(\angle C) \sin(\varphi(r_V)) - \sin(\angle C) \cos(\varphi(r_V))] u_0 \\ & + |C|^2 \left(\frac{4R_A}{\pi\omega^2} \right)^2 = (|C|w_0)^2. \end{aligned} \quad (76)$$

An alternative approach to the solution of the above equation is to consider that, in correspondence of the supercritical fold point, the derivative of u_0 with respect to ω must be

$$\frac{du_0}{d\omega} \rightarrow \infty, \quad (77)$$

as clearly shown in Fig. 20. To exploit this property, let us consider the derivative of the left- and right-hand sides of

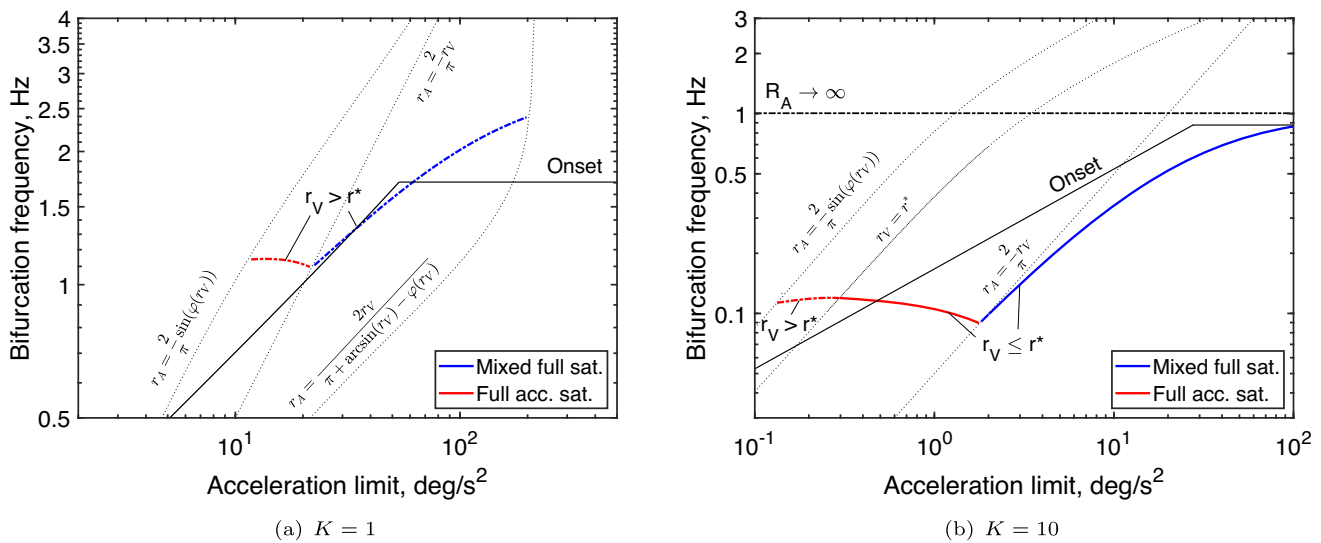


Fig. 22 Bifurcation frequency of a first-order closed-loop system for $w_0 = 1$ deg, $R_V = 5$ deg/s and varying acceleration limit

Eq.(76) with respect to ω and neglect finite terms, obtaining

$$u_0 \frac{du_0}{d\omega} + \frac{8}{\pi} |C| \frac{R_A}{\omega^2} \left[\cos(\angle C) \frac{d}{d\omega} (u_0 \sin(\varphi(r_V))) - \sin(\angle C) \frac{d}{d\omega} (u_0 \cos(\varphi(r_V))) \right] = 0 \quad (78)$$

In order to solve the above equation, the derivative

$$\frac{d\varphi(r_V)}{d\omega} = \frac{d\varphi(r_V)}{dr_V} \frac{dr_V}{d\omega} \quad (79)$$

must be evaluated. From the definition of $\varphi(r_V)$ in Eq.(9), it can be obtained that

$$\frac{d\varphi(r_V)}{dr_V} = \frac{\sin^{-1}(r_V) - \varphi(r_V)}{r_V - \sin(\varphi(r_V))}, \quad (80)$$

while, from the definition of r_V in Eq.(4), deriving with respect to ω and cancelling finite terms, it results that

$$\frac{dr_V}{d\omega} \cong -\frac{r_V}{u_0} \frac{du_0}{d\omega}. \quad (81)$$

Therefore, substituting Eqs.(80) and (81), Eq.(79) yields

$$\frac{d\varphi(r_V)}{d\omega} = -\frac{r_V \sin^{-1}(r_V) - \varphi(r_V)}{u_0} \frac{du_0}{d\omega} \quad (82)$$

Replacing Eq.(82) into Eq.(76), after some algebraic manipulations, it is derived that, at the supercritical fold point,

$$u_{0,b} = \frac{4R_A}{\pi \omega^2} |C(j\omega_b)| \Theta(j\omega_b, r_{V,b}), \quad (83)$$

where

$$\Theta(j\omega, r_V) = \frac{1}{r_V - \sin(\varphi(r_V))} \left[\cos(\angle C(j\omega)) - \cos(\angle C(j\omega) + \sin^{-1}(r_V) - \varphi(r_V)) \right], \quad (84)$$

and

$$\omega_b^2 = \frac{4R_A}{\pi w_0} \cdot \sqrt{1 + \Theta_b^2 - 2\Theta_b \sin(\angle C(j\omega_b) - \varphi(r_{V,b}))}. \quad (85)$$

The bifurcation frequency can be similarly derived in mixed full saturation regime, resulting in

$$\omega_b^2 = \frac{4R_A}{\pi w_0} \sin\left(\frac{R_V}{R_A} \omega_b\right) \cdot \sqrt{1 + \Theta_b'^2 - 2\Theta_b' \cos(\angle C(j\omega_b) - \frac{R_V}{R_A} \omega_b - \varphi(r_{V,b}))}, \quad (86)$$

where

$$\Theta'(j\omega, r_V) = \frac{1}{r_V - \sin(\varphi(r_V))} \cdot \left[\sin\left(\angle C(j\omega) - \frac{R_V}{R_A} \omega + \sin^{-1}(r_V) - \varphi(r_V)\right) - \sin\left(\angle C(j\omega) - \frac{R_V}{R_A} \omega\right) \right], \quad (87)$$

while the corresponding amplitude u_0 can be written as

$$u_{0,b} = \frac{4R_A}{\pi\omega_b^2} \sin\left(\frac{R_V}{R_A}\omega_b\right) |C(j\omega_b)|\Theta'_b. \quad (88)$$

In both saturation regimes, the validity of the solution can be verified by referring to the boundaries derived in Sect. 2. It is worth underlining that the solutions obtained for $r^* < r_V < 1$ depend on both frequency and rate limit ratio, with the latter depending on the frequency itself and amplitude u_0 . Therefore, a constrained nonlinear optimisation algorithm, implemented through the Matlab function *fmincon* [37], was used in this paper to solve Eqs. (85) and (86).

The above formulations have been applied to the case-studies investigated in this section, setting $w_0 = 1$ deg, $R_V = 5$ deg/s and varying acceleration limit. In the case $K = 1$ (shown in Fig. 22a), for which rate limit cannot lead to jump resonance in the absence of acceleration limits, solutions have been found in a limited range of the acceleration limit, included between 11.8 and 198 deg/s². This result is consistent with the behaviour shown in Figs. 18 and 19, where jump resonance is not observed for $R_A = 10$ and 200 deg/s². In agreement with these previous results, all supercritical folds occur for $r^* < r_V < 1$, either in full mixed or acceleration saturation regimes. For $K = 10$, as shown in Fig. 22b, jump resonance occurs for any acceleration limit larger than 0.13 deg/s², with the bifurcation frequency approaching the value observed in the absence of acceleration limits when $R_A \rightarrow \infty$. In this case, supercritical folds take place at $r_V \leq r^*$ for most acceleration limit values. It has been observed that jump resonances starting at $r_V \leq r^*$ are generally more severe, since they tend to generate larger jumps between different solution branches and are therefore more likely to lead to dynamic instability.

5 Application to a high-order aeroservoelastic model for gust load alleviation

In this section, the describing function framework developed in the previous sections is applied to the analysis of actuator rate and acceleration limit effects in a high-order aeroservoelastic control system. The case study considered corresponds to a gust load alleviation (GLA) configuration investigated by the authors' previous contribution [34], and is used here to illustrate the applicability and limitations of the proposed analytical approach.

The purpose of this investigation is not to provide a comprehensive nonlinear validation of the aeroservoelastic model, but rather to use it as a representative example to discuss how actuator rate and acceleration limits modify the effective closed-loop dynamics and, ultimately, the control

function performance. In particular, two parametric studies are considered: (i) the effect of varying the actuator rate limit, and (ii) the effect of varying the acceleration limit for a fixed rate limit. For each case, the effect of actuator nonlinearities on closed-loop dynamics is determined by first evaluating the onset frequency of the nonlinearity and the supercritical fold frequency of jump resonance, and then the equivalent describing function of the feedback loop and the frequency spectrum of the wing structural response, expressed by the wing-root bending moment (WRBM).

5.1 System definition

The aeroelastic model represents a flexible wing with unsteady aerodynamics and consists of a linear state-space realization of 96 states. For control design and analysis purposes, the model has been reduced using balanced truncation, resulting in a 35-state representation that accurately preserves the low-frequency aeroelastic dynamics relevant to GLA. The reduced-order model is augmented with a first-order actuator model governed by the transfer function

$$C(s) = \frac{\omega_a}{s + \omega_a}. \quad (89)$$

with $\omega_a = 90$ rad/s. A linear quadratic regulator (LQR) is designed based on the reduced-order linear model and the additional actuator internal state, with the objective of mitigating gust-induced wing root bending moments using an outboard aileron. Owing to the relatively high frequency of the first aeroelastic mode (about 19.7 Hz), the closed-loop system exhibits significant sensitivity to actuator dynamics and limitations, making it a suitable test case for the investigation of frequency-dependent nonlinear effects.

To enable the application of the proposed describing function approach, the actuator rate and/or acceleration limits are replaced with their describing function, derived in Sect. 3, and equivalent single-input single-output (SISO) linear models are used to represent the remaining elements of the feedback loop, as schematically represented in Fig. 23. In particular, the multi-input multi-output aeroelastic plant and the LQR controller are reduced to the SISO transfer functions G_u and G_w , respectively mapping the actuator output u_N and the gust perturbation w into the demanded aileron deflection z . The current analysis is restricted to the case of sinusoidal gust excitation, with amplitude set to $w_0 = 4.2472$ m/s, corresponding to a gust angle of attack of 0.9682 degrees. Finally, it is assumed that no further aileron deflection is commanded externally ($r = 0$).

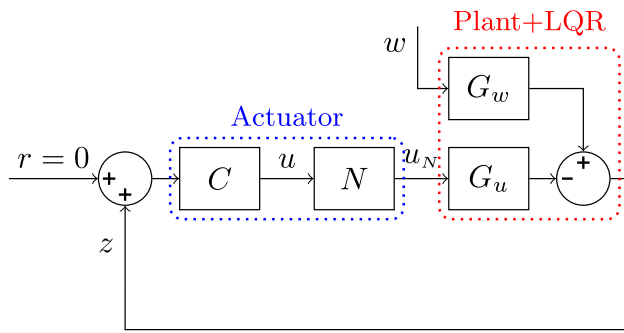


Fig. 23 Schematic representation of the gust load alleviation feedback loop

5.2 Effect of actuator rate limit

The proposed describing function approach is first applied to the system introduced in the above subsection to evaluate the effect of varying actuator rate limit, assuming no limitations for the achievable acceleration ($R_A \rightarrow \infty$). As a first step, the closed-loop onset frequency of the rate limit is calculated from Eq.(47), setting

$$\frac{u}{w}(j\omega) = \frac{G_w(j\omega)}{1 + C(j\omega)G_u(j\omega)} \quad (90)$$

as the linear transfer function between the gust input $w(t)$ and the rate limit input $u(t)$. The resulting evolution of the onset frequency $\tilde{\omega}_V$ for varying rate limit values is represented in Fig. 24. It is possible to observe that, for rate limits up to about 400 deg/s, the onset frequency increases almost linearly with R_V , in a similar fashion to the first-order case presented in Sect. 4.3. However, for larger values of the rate limit, the onset of the nonlinearity occurs at frequencies that are in the range of the plant dynamics. This can result in multiple transitions between linear to nonlinear behaviour, with the latter mostly affecting the resonant peaks of the closed-loop system, activated by larger response amplitudes.

The occurrence of jump resonance induced by the actuator rate limit can be investigated by adapting the analytical formulations derived in Sect. 4.4.1 for first-order systems to the present case study. The presence of jump resonance is first verified from Eq.(69), substituting $C(j\omega)G_u(j\omega)$ in place of $C(j\omega)$. When jump resonance is predicted to occur, the corresponding supercritical fold frequency can then be evaluated from an updated formulation of Eq.(68), which reads as

$$\omega_b = \frac{\pi R_V}{2|C G_w(j\omega_b)|w_0} \left| 1 + \frac{8}{\pi^2} \operatorname{Re}\{C G_u(j\omega_b)\} \right|. \quad (91)$$

The resulting predictions for jump resonance are reported in Fig. 24, along with the closed-loop onset frequency. It can be observed that jump resonance takes place for rate limits

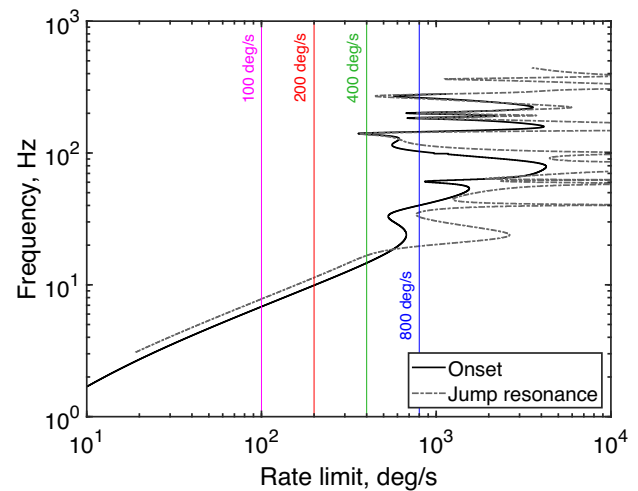


Fig. 24 Onset and bifurcation frequencies of the aeroservoelastic system for varying rate limits

above 18.6 deg/s. For rate limit values up to about 400 deg/s, the supercritical fold frequency presents a regular pattern, increasing almost linearly with the rate limit, and is characterised by slightly larger frequency values than the onset point, indicating that jump resonance occurs soon after the rate limit onset. For larger values of the rate limit, where the interaction with the frequency content of the plant dynamics becomes evident, irregular behaviour and multiple jump resonances can be observed. It is noteworthy that not only is the jump resonance predicted to occur at lower frequencies than the rate limit onset, but also multiple folding frequencies are found below the onset frequency. This behaviour is explained in the remainder of this subsection. Finally, an upper bound for the occurrence of jump resonance is found at $R_V \cong 1.8 \cdot 10^6$ deg/s. However, for very large rate limits, it can be reasonably assumed that such effects are minimal and only affect resonant peaks, with little impact on the overall dynamics of the system.

The effect of actuator rate limits on the frequency response of the aeroservoelastic system, studied by considering the describing function of the rate limit derived in Sect. 3.1 and the approach described in Sect. 4.2, is illustrated in Fig. 25, where the input and output signal amplitudes of the rate limit element, the equivalent open-loop describing function, and the resulting WRBM are reported for varying sinusoidal gust excitation frequencies and rate limits equal to 100, 200, 400, and 800 deg/s. It can be observed that the rate limit strongly affects the closed-loop dynamics. In particular, rate saturation leads to a reduction in the output actuator deflection amplitude, which becomes gradually more severe at high frequencies. As a result, the WRBMs generated by the control function are no longer sufficient to fully compensate the gust loads. In this context, the actuator deflection demanded by the controller increases dramatically, eventually leading

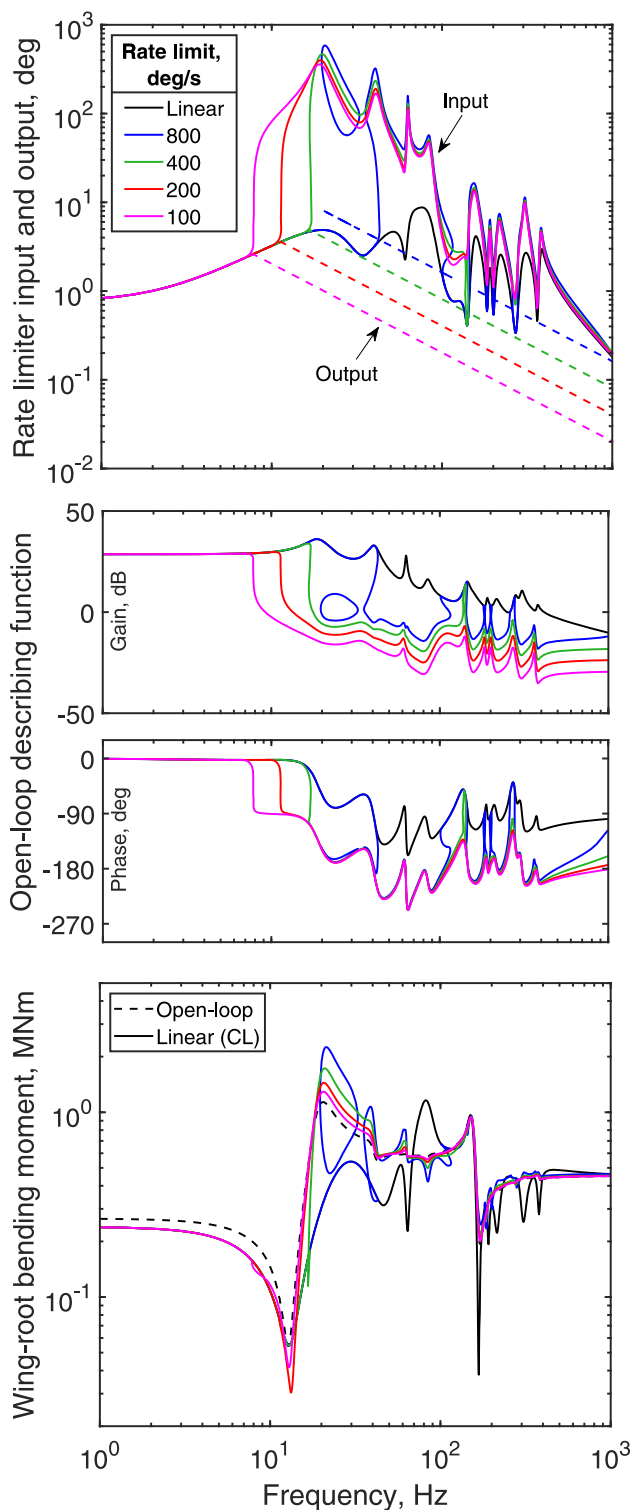


Fig. 25 Input and output of the nonlinear element, open-loop describing function and wing-root bending moment for varying sinusoidal excitation frequencies and rate limits

to jump resonance. For rate limit values up to 400 deg/s, in agreement with the behaviour described in Fig. 24, jump resonance occurs soon after the onset of nonlinear behaviour

and is associated with a sudden and significant increase in the demanded actuator deflection, together with a drastic decrease in the control functionality, eventually leading to output WRBMs that may even exceed those of the open-loop, uncontrolled system. Very distinct dynamic behaviour is observed for $R_V = 800$ deg/s. In this case, the less severe rate limitation leads to a higher onset frequency, larger than that of the first aeroelastic mode, which is therefore effectively controlled. However, it is observed that jump resonance produces isolated nonlinear solution branches. This type of jump resonance has already been reported in the literature [32], and is consistently predicted by the analytical procedure proposed in this paper. In fact, three solutions for the bifurcation frequency are found for $R_V = 800$ deg/s, as visible in Fig. 24; the first two of these solutions are associated with the lowest and highest frequencies of the isolated branch, while the third corresponds to the supercritical fold frequency of the subsequent jump, occurring in proximity to the rate limit onset on the main solution branch. It can therefore be concluded that, in the presence of actuator rate limits, sudden jumps to large-amplitude nonlinear solutions may be triggered by external perturbations even when the actuator is operating in a linear regime.

5.3 Effect of combined actuator rate and acceleration limits

The combined effect of actuator rate and acceleration limits is investigated with the proposed describing function approach for $R_V = 400$ deg/s and varying acceleration limits. The closed-loop onset frequency is evaluated by replacing Eq.(90) into Eqs.(47) and (49), and its variation with R_A is shown in Fig. 26. It is possible to observe that the onset frequency of the nonlinear behaviour increases with R_A approximately following a quadratic law in the range where the onset is governed by the acceleration limit, up to $R_A \cong 3.6$ deg/s². For larger values of the acceleration limit, the onset is instead governed by the rate limit, and assumes the constant value of 14.65 Hz. Since this frequency is well below the first resonant frequency of the aeroelastic plant, the evolution of the closed-loop onset frequencies closely resembles that observed for the first-order system in Sect. 4.

The occurrence of jump resonance and the corresponding supercritical fold frequencies are evaluated adapting the analytical formulations derived in Sect. 4.4.2 to the aeroservoelastic system under investigation, with results reported in Fig. 26. It can be observed that jump resonance is predicted to occur for any acceleration limit larger than 2.80 deg/s². As for the onset frequency, the evolution of the bifurcation frequency mimics that observed for first-order systems (see Fig. 22b), since jump resonance occurs below the first resonant frequency of the aeroelastic plant. For smaller values of the acceleration limit, jump resonance occurs in full satu-

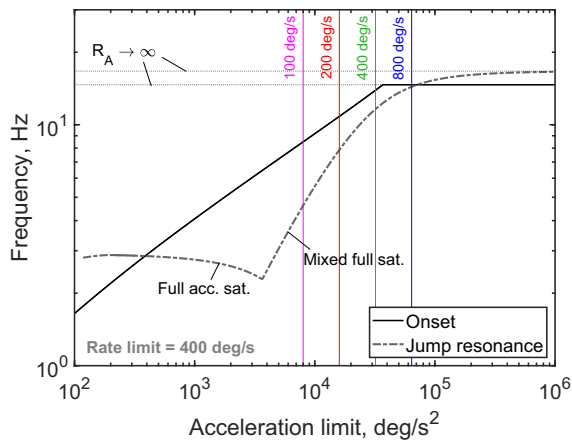


Fig. 26 Onset and bifurcation frequencies of the aeroservoelastic system for $R_V = 400$ deg/s and varying acceleration rate limits

ration regime, and the supercritical fold frequency decreases with R_A until a minimum of equal to 2.28 Hz is reached at $R_A = 3620$ deg/s². For larger acceleration limits, the bifurcation frequency gradually increases, eventually reaching the value of 16.7 Hz observed in the presence of rate limit only. It is noteworthy that jump resonance occurs significantly below the onset point for a wide range of acceleration limits.

The combined effect of actuator rate and acceleration limits on the frequency response has been explored by substituting the describing function formulations derived in Sect. 3.3 and following the procedure described in Sect. 4.2. The input and output signal amplitudes of the nonlinear element, the open-loop describing function of the feedback loop and the output WRBM are illustrated in Fig. 27 for $R_V = 400$ deg/s and acceleration limits equal to 8000, 16000, 32000, and 64000 deg/s². It can be observed that the introduction of acceleration limits leads not only to an earlier onset of the nonlinear behaviour, but also to a strong decrease in the supercritical fold frequency of jump resonances, consistently with the pattern anticipated by Fig. 26. Therefore, in the presence of strict acceleration limits, jumps may occur between linear and nonlinear solution branches under the action of sufficiently large perturbations, leading to sudden loss of control functionality and potential dynamic instability.

5.4 Scope and limitations of describing function framework

The results presented in this section also highlight the scope and limitations of the describing function approach adopted in this work. Describing functions provide an approximate frequency-domain representation of nonlinear elements and are primarily intended to predict the onset of nonlinear behaviour, the existence of multiple periodic solutions and the occurrence of jump resonance through fold bifurcations.

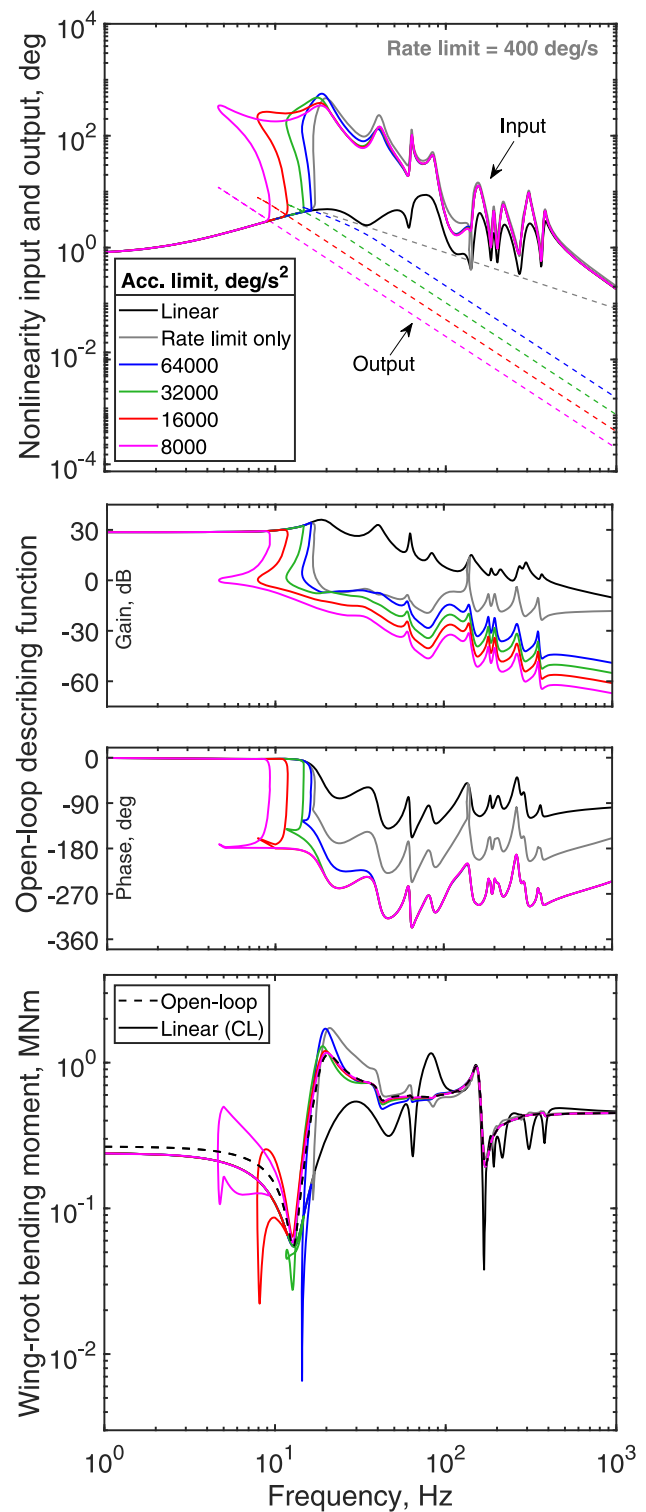


Fig. 27 Input and output of the nonlinearity, open-loop describing function and wing-root bending moment for $R_V = 400$ deg/s, varying excitation frequencies and acceleration limits

As such, the analysis relies on an accurate representation of the closed-loop frequency response in the vicinity of the pre-

dicted onset and bifurcation frequencies, rather than on a fully accurate time-domain model of the system. Moderate modelling uncertainties may affect the quantitative prediction of critical frequencies, but do not alter the qualitative trends identified by the analysis, such as the presence of solution multiplicity and abrupt transitions in the system response. The reliability of the describing function approximation is highest when nonlinear effects develop at frequencies well separated from higher-order resonances of the underlying linear plant. At higher frequencies, where actuator nonlinearities generate significant higher-harmonic content and interact with complex aeroelastic dynamics, the describing function should be regarded as an indicator of potentially critical operating regions rather than as a definitive predictor of stability. A complete assessment of nonlinear stability and transient behaviour in these regimes requires time-domain analysis, which is beyond the scope of the present work.

6 Conclusions

In this paper, the nonlinear dynamic effects introduced by actuator rate and acceleration limits in closed-loop systems were analysed. A full characterisation of the saturation regimes determined by these nonlinearities in the steady-state actuator response to sinusoidal input was presented, along with the analytical derivation of the conditions for the transitions between different regimes. The boundaries between saturation regimes were represented in a two-dimensional parameter space defined by non-dimensionalised rate and acceleration limits, enabling the prediction of saturation regime based on the input amplitude and frequency.

Analytical expressions for the describing functions of rate, acceleration, and combined rate-acceleration limits were derived in each regime. These describing functions capture the input–output relationship of the actuator in the frequency domain and provide a basis for understanding the dynamics of closed-loop systems, where they allowed for the evaluation of the nonlinearity onset and the determination of an equivalent describing function for the feedback loop. Moreover, these describing functions enabled the analytical derivation of the conditions for the existence of nonlinear jump resonances and the corresponding supercritical fold frequencies (the lowest frequencies at which multiple steady-state solutions coexist).

The investigation showed that various types of steady-state responses may arise under sinusoidal excitation when either or both rate and acceleration limits are active, including full or partial saturation of these quantities. When both limits are applied, strict acceleration limits can conceal the presence of a rate limit, due to their leading effect on the response amplitude. In fact, the describing function analysis demonstrated that acceleration limits introduce a stronger attenuation, with

a -40 dB/decade gain reduction at high frequencies, independently of the presence of rate limits, while rate limits alone result in a -20 dB/decade slope. In addition, it was observed that the closed-loop output amplitude at high frequencies depends only on the actuator input amplitude and the nonlinear limits, while being independent of the linear system dynamics. This feature could facilitate the identification of actuator limits via high-frequency experiments, even when the plant dynamics are uncertain.

Combined rate and acceleration limits also have a pronounced impact on phase behaviour. In particular, the actuator input–output phase lag approaches 180 degrees at high frequencies, conversely to the 90 degrees lag observed when only one limit is active. This phase shift also appears in the closed-loop system, although there it is also affected by the linear dynamics of the system. Furthermore, describing function phase curves often exhibit nonsmooth transitions and angular points near regime transitions, especially in the presence of acceleration limits. These features underscore the limitations of adopting interpolation (e.g., cubic splines) to reconstruct partial saturation dynamics and the value of the full analytical formulation derived in this work.

In closed-loop systems, nonlinear jump resonances were shown to arise under either rate or combined rate–acceleration limits, producing multiple steady-state solutions over specific frequency ranges. These phenomena can cause abrupt changes in system response and potentially lead to loss of stability. Moreover, nonlinear solution branches may extend to frequencies below the onset point, indicating that, even when the actuator operates predominantly in a linear regime, the system may exhibit sudden transitions due to latent nonlinear dynamics. These effects were explicitly demonstrated through the application of the proposed framework to a high-order aeroservoelastic model for gust load alleviation, where the interaction between actuator nonlinearities and the closed-loop aeroelastic dynamics was shown to produce multiple jump resonance scenarios and isolated nonlinear response branches. Acceleration limits were found to induce similar jump phenomena even when rate limits alone would not, or to further extend nonlinear branches already caused by rate saturation. In particular, the analysis revealed that acceleration constraints can significantly lower the frequencies at which jump resonances occur and exacerbate their impact on control effectiveness, highlighting the critical role of acceleration limits in high-bandwidth control applications.

Overall, the results offer a comprehensive framework for analysing the impact of actuator rate and acceleration limits on closed-loop system dynamics. The insights into steady-state regimes, describing function behaviour and jump resonance conditions are particularly relevant for preliminary design and frequency-domain stability assessment of control systems, with direct applicability to high-bandwidth actua-

tion problems across a range of engineering domains. While the present study focuses on steady-state and frequency-domain characterisation, a rigorous assessment of nonlinear stability and transient behaviour requires time-domain analysis, which is beyond the scope of this work and will be addressed by the authors in a separate publication.

Acknowledgements The authors are grateful to Dr Xuerui Wang for helpful discussions and for providing feedback on an initial version of this manuscript.

Author Contributions Luca Marino: Conceptualization, Formal analysis, Investigation, Methodology, Writing - original draft, Writing - review & editing. Jurij Sodja: Conceptualization, Funding acquisition, Supervision.

Funding This research has been performed in the frame of the CONCERTO project (Construction Of Novel CERTification methOds and means of compliance for disruptive technologies), which is funded by the European Community's Clean Aviation Joint Undertaking programme, under Grant Agreement No 101101999. The project started on January 1, 2023.



Data Availability Data are contained within the article.

Declarations

Conflict of interest The authors have no relevant financial or non-financial interests to disclose.

Competing interests The authors declare no competing interests.

Disclaimer Co-Funded by the European Union. Views and opinions expressed are however those of the authors only and do not necessarily reflect those of the European Union or Clean Aviation Joint Undertaking. Neither the European Union nor the granting authority can be held responsible for them.

Open Access This article is licensed under a Creative Commons Attribution 4.0 International License, which permits use, sharing, adaptation, distribution and reproduction in any medium or format, as long as you give appropriate credit to the original author(s) and the source, provide a link to the Creative Commons licence, and indicate if changes were made. The images or other third party material in this article are included in the article's Creative Commons licence, unless indicated otherwise in a credit line to the material. If material is not included in the article's Creative Commons licence and your intended use is not permitted by statutory regulation or exceeds the permitted use, you will need to obtain permission directly from the copyright holder. To view a copy of this licence, visit <http://creativecommons.org/licenses/by/4.0/>.

References

- Du, H., Zhang, N., Naghdy, F.: Actuator saturation control of uncertain structures with input time delay. *J. Sound Vib.* **330**(18–19), 4399–4412 (2011). <https://doi.org/10.1016/j.jsv.2011.04.025>
- Ding, Y., Weng, F., Yu, Z.: Actuator saturation and control design for buildings structural systems with improved uncertainty description. *Shock. Vib.* **20**(2), 297–308 (2013). <https://doi.org/10.3233/SAV-2012-00745>
- Huang, S., Cai, M., Xiang, Z.: Robust sampled-data H_∞ control for offshore platforms subject to irregular wave forces and actuator saturation. *Nonlinear Dyn.* **88**(4), 2705–2721 (2017). <https://doi.org/10.1007/s11071-017-3404-6>
- Gao, H., Sun, W., Shi, P.: Robust sampled-data H_∞ control for vehicle active suspension systems. *IEEE Trans. Control Syst. Technol.* **18**(1), 238–245 (2010). <https://doi.org/10.1109/TCST.2009.2015653>
- Zhao, Y.: Robust control synthesis for seat suspension systems with actuator saturation and time-varying input delay. *J. Sound Vib.* **329**(21), 4335–4353 (2010). <https://doi.org/10.1016/j.jsv.2009.09.017>
- Xia, K., Zou, Y.: Adaptive saturated fault-tolerant control for spacecraft rendezvous with redundancy thrusters. *IEEE Trans. Control Syst. Technol.* **29**(2), 502–513 (2021). <https://doi.org/10.1109/TCST.2019.2950399>
- Hosseinnajad, A., Loueipour, M.: Velocity-based tuning of degree of homogeneity for finite-time stabilization and fault tolerant control of an ROV in the presence of thruster saturation and rate limits. *Nonlinear Dyn.* **111**(5), 8253–8274 (2023). <https://doi.org/10.1007/s11071-022-08222-8>
- Shojaei, K.: Output-feedback formation control of wheeled mobile robots with actuators saturation compensation. *Nonlinear Dyn.* **89**, 2867–2878 (2017). <https://doi.org/10.1007/s11071-017-3631-x>
- Duda, H.: Frequency domain analysis of rate limiting elements in flight control systems, pp. 94–16. Tech. rep, DLR-FB (1994)
- Gilbreath, G.: Prediction of pilot-induced oscillations due to actuator rate limiting using the open-loop onset point criterion. Tech. rep, Air Force Institute of Technology, Wright-Patterson Air Force Base, OH (2001)
- Shifrin, C.: Sweden seeks cause of gripen crash. *Aviation Week Space Technol.* **139**(7), 78–79 (1993)
- McRuer, D.: National Research Council: Aviation Safety and Pilot Control: Understanding and Preventing Unfavorable Pilot-Vehicle Interactions. The National Academies Press, Washington, DC (1997)
- Duda, H.: Flight control system design considering rate saturation. *Aerosp. Sci. Technol.* **2**(4), 265–275 (1998). [https://doi.org/10.1016/S1270-9638\(98\)80004-7](https://doi.org/10.1016/S1270-9638(98)80004-7)
- Tang, M., Böswald, M., Govers, Y., Pusch, M.: Identification and assessment of a nonlinear dynamic actuator model for gust load alleviation in a wind tunnel experiment, In: Deutscher Luft- und Raumfahrtkongress (2019)
- Tang, M., Böswald, M., Govers, Y., Pusch, M.: Identification and assessment of a nonlinear dynamic actuator model for controlling an experimental flexible wing. *CEAS Aeronaut. J.* **12**, 413–426 (2021). <https://doi.org/10.1007/s13272-021-00504-y>
- Micheli, B.: Active flutter suppression: Quantification of performance loss due to actuator saturation. *J. Guid. Control. Dyn.* **47**(1), 2333–2350 (2024). <https://doi.org/10.2514/1.G008146>
- Theis, J., Pfifer, H., Seiler, P.: Robust control design for active flutter suppression, In: AIAA Atmospheric Flight Mechanics Conference, p. 1751. (2016) <https://doi.org/10.2514/6.2016-1751>
- Pusch, M., Ossmann, D., Luspäy, T.: Structured control design for a highly flexible flutter demonstrator. *Aerosp.* **6**(3), 7 (2019). <https://doi.org/10.3390/aerospace6030027>
- Fielding, C., Flux, P.: Non-linearities in flight control systems. *Aeronaut. J.* **107**(1077), 673–696 (2003). <https://doi.org/10.1017/S0001924000013543>
- Yuan, J., Fei, S., Chen, Y.: Compensation strategies based on bode step concept for actuator rate limit effect on first-order plus time-

- delay systems. *Nonlinear Dyn.* **99**(2), 2851–2866 (2020). <https://doi.org/10.1007/s11071-019-05454-z>
21. Gelb, A., Vander Velde, W.: *Multiple-Input Describing Functions and Nonlinear System Design* (McGraw-Hill, New York, NY, 1968)
 22. Roberge, J.: *Operational Amplifiers: Theory and Practice* (Wiley & Sons, 1975)
 23. Slotine, J.J., Li, W.: *Applied Nonlinear Control*. Prentice-Hall International Editions, Englewood Cliffs, NJ (1991)
 24. Hanke, D.: Handling qualities analysis on rate limiting elements in flight control systems, In: *Flight Vehicle Integration Panel Workshop in Pilot Induced Oscillations*, AGARD-AR-335 (1995)
 25. Román, M., Ponce, E.: The describing function method accuracy in first order plants with rate-limited feedback. 2003 European Control Conference (ECC), Cambridge, UK pp. 1620–1625 (2003). <https://doi.org/10.23919/ECC.2003.7085195>
 26. Ponce, E., Roman, M.: Limit cycle bifurcation induced by rate-limiters in the feedback loop. *IFAC Proceedings Volumes* **39**(8), 209–214 (2006). <https://doi.org/10.3182/20060628-3-FR-3903.00038>
 27. Tavakkoli, F., Khosravi, A., Sarhadi, P.: Robustness analysis of model reference adaptive control in the presence of input rate saturation using the describing function method. *Int. J. Dyn. Control* **12**(1), 1415–1426 (2024). <https://doi.org/10.1007/s40435-023-01184-8>
 28. Amato, F., Iervolino, R., Pandit, M., Scala, S., Verde, L.: Analysis of pilot-in-the-loop oscillations due to position and rate saturations, In: *Proc. 39th IEEE Conf. Decis. Control.*, vol. 4, p. 3564–3569. (2000) <https://doi.org/10.1109/CDC.2000.912258>
 29. Meng, J., Xu, H., Zhang, J.: A comparison of rate-limit phase compensator to prevent category II pilot induced oscillations, In: *Proceedings of the 8th World Congress on Intelligent Control and Automation*, p. 3872–3877. (2010) <https://doi.org/10.1109/WCICA.2010.5555356>
 30. Alstrom, R., Bollt, E., Marzocca, P., Ahmadi, G.: The application of nonlinear pre-filters to prevent aeroservoelastic interactions due to actuator rate limiting, in *Proceedings of the 53rd AIAA/ASME/ASCE/AHS/ASC Structures, Structural Dynamics and Materials Conference* (2012). <https://doi.org/10.2514/6.2012-1483>
 31. Katayanagi, R.: Pilot-induced oscillation analysis with actuator rate limiting and feedback control loop. *Trans. Jpn. Soc. Aeronaut. Space Sci.* **44**(143), 48–53 (2001). <https://doi.org/10.2322/tjsass.44.48>
 32. Fukuma, A., Matsubara, M.: Jump resonance in nonlinear feedback systems — part i: Approximate analysis by the describing-function methods. *IEEE Trans. Autom. Contr.* **23**, 891–896 (1978). <https://doi.org/10.1109/TAC.1978.1101876>
 33. Hsu, J., Meyer, A.: *Modern control principles and applications* (McGraw-Hill, 1968)
 34. Marino, L., Wang, X., Sodja, J.: Nonlinear analysis of combined rate and acceleration limits effect on actuator performance, In: *International Forum on Aeroelasticity and Structural Dynamics 2024*, pp. IFASD–2024–183. (2024) <https://doi.org/10.82439/ceas-ifasd-2024-183>
 35. Nakabayashi, Y., Okajima, H., Matsunaga, N.: Signal limitation filter to satisfy velocity and acceleration constraints for arbitrary input signals, In: *Proceedings of the 56th Annual Conference of the Society of Instrument and Control Engineers of Japan*, pp. 1197–1201. (2017) <https://doi.org/10.23919/SICE.2017.8105481>
 36. Tombul, G.: Simultaneous feedforward online command rate limiter filters for existing controllers. *Turk. J. Elec. Eng. Comp. Sci.* **29**(5), 2529–2544 (2021). <https://doi.org/10.3906/elk-2007-147>
 37. MATLAB, Optimization Toolbox: `fmincon`. The MathWorks, Inc., Natick, Massachusetts, United States (2024). <https://www.mathworks.com/help/optim/ug/fmincon.html>. Accessed: 2025-06-16

Publisher's Note Springer Nature remains neutral with regard to jurisdictional claims in published maps and institutional affiliations.